Modification of Nickel Foam as highly active and stable bifunctional electrode material for industrial water splitting

MD AMIRUL MOMININ

SUPERVISOR
Foysal Kabir Tareq
Souman Rudra
Sajal Chandra Banik

University of Agder, [2024]
Faculty of Engineering and Science
Department of Engineering Sciences

Abstract

Renewable energy offers the potential for a sustainable and eco-friendly energy future for the planet. Solar, wind, hydropower, biofuels, and other renewable energy sources are the key drivers of the shift toward green energy systems that aggregated a significant expansion in their generation capacity in recent years. In addition, hydrogen is a versatile energy carrier and storage medium known for its high energy density of 141.9 MJ/kg . Due to its non-polluting properties and synthesis opportunity from earth abundance water, hydrogen became one of the most attractive sources of energy in future. Electrochemical water splitting is the key process which encompasses the critical reaction hydrogen evolution reaction (HER) and oxygen evolution reaction (OER) to produce clean hydrogen using external energy sources. To produce hydrogen at low cost, stable and cheap electrocatalyst is needed. To progress the advancement of highly active, efficient and low cost electrocatalyst, nickel foam is chosen for thermal treatment varying duration as it is a promising non-noble substrate material exhibits excellent conductivity and robust mechanical properties. It is found in this study that nickel foam is annealed at 600° C for one hour shows overpotential of 377 mV at current density 10mA/cm^2 for OER and annealed at 500° C for half an hour shows the best performance among samples for HER with overpotential 146mV at 10 mA/cm^2 under 1.0 M KOH alkaline condition, due to the resulted combination of porous hole and nickel oxide active sites. In addition, produced electrodes show excellent full cell performance in industrial water splitting condition in 6.0 M KOH solution with only 2.33 V_{cell} to achieve 500 mA/cm^2 and exhibits stable long-term durability. The simplicity of synthesis process makes it highly reproducible to overcome the challenges in hydrogen production due to high-cost noble metal catalysts, limited stability and complex synthesis process.

Sammendrag

Fornybar energi tilbyr potensialet for en bærekraftig og miljøvennlig energifremtid for planeten. Solenergi, vindkraft, vannkraft, biodrivstoff og andre fornybare energikilder er de viktigste drivkreftene bak overgangen til grønne energisystemer, som har opplevd en betydelig økning i produksjonskapasitet de siste årene. I tillegg er hydrogen en allsidig energibærer og lagringsmedium kjent for sin høye energitetthet på 141,9 MJ/kg. På grunn av sine ikke-forurensende egenskaper og muligheten for syntese fra vann, som finnes i overflod på jorden, har hydrogen blitt en av de mest attraktive energikildene for fremtiden. Elektrolytisk vannspalting er en nøkkelprosess som inkluderer de kritiske reaksjonene hydrogenevolusjonsreaksjonen (HER) og oksygenevolusjonsreaksjonen (OER) for å produsere rent hydrogen ved hjelp av eksterne energikilder. For å produsere hydrogen til lav kostnad er det nødvendig med en stabil og rimelig elektrokatalysator. For å fremme utviklingen av svært aktive, effektive og kostnadseffektive elektrokatalysatorer, ble nikkelskum valgt for termisk behandling over varierende tidsperioder, ettersom det er et lovende ikke-eddelt substratmateriale som viser utmerket ledningsevne og robuste mekaniske egenskaper. Det ble funnet i denne studien at nikkelskum som ble glødet ved 600 °C i én time, oppnår et overpotensial på 377 mV ved en strømtetthet på 10 mA/cm² for OER, og at skum glødet ved 500 °C i en halv time viser den beste ytelsen blant prøvene for HER med et overpotensial på 146 mV ved 10 mA/cm² under 1,0 M KOH-alkaliske forhold. Dette skyldes den resulterende kombinasjonen av porøse hull og aktive nikkeloksidsteder. I tillegg viser de produserte elektrodene utmerket ytelse i full celle under industrielle vannspaltningsforhold i en 6,0 M KOH-løsning, med kun 2,33 Vcelle nødvendig for å oppnå 500 mA/cm², og de utviser stabil langvarig holdbarhet. Enkelheten i synteseprosessen gjør den svært reproduserbar og i stand til å overvinne utfordringene ved hydrogenproduksjon, som høykostnads-eddelmetallkatalysatorer, begrenset stabilitet og komplekse synteseprosesser.

Preface

This thesis work was conducted in autumn 2024 under the project "Collaborative Action for Improving Educational Capacities in Renewable Energy to mitigate climate crisis (CARE)" between Chittagong University of Engineering & Technology (CUET), Bangladesh and the University of Agder (UiA), Norway (Collaboration Agreement No. NORPART-2021/10355).

I would like to express my sincere gratitude to my supervisors, Foysal Kabir Tareq and Prof. Souman Rudra, for their invaluable guidance, supervision and excellent advice throughout the project. I am also thankful to Prof. Sajal Chandra Banik and Prof. Abu Shadat Mohammad Sayem for their mentorship, guidance and motivation during this thesis work.

I want to express my deepest gratitude to my father, mother and wife for their unwavering support and encouragement to pursue this thesis in UiA, Norway.

I want to express my heartfelt appreciation to Md Iftekhar Hossain and others for their assistance with their technical expertise, information and motivation that helped me a lot to conclude this work.

Md Amirul Mominin
University of Agder, Norway
Grimstad, December 2024

Individual/group Mandatory Declaration

The individual student or group of students is responsible for the use of legal tools, guidelines for using these and rules on source usage. The statement will make the students aware of their responsibilities and the consequences of cheating. Missing statement does not release students from their responsibility.

1.	I/We hereby declare that my/our report is my/our own work and that I/We have not used any other sources or have received any other help than mentioned in the thesis.	☒
2.	I/we further declare that this thesis: - has not been used for another exam at another department/university/university college in Norway or abroad; - does not refer to the work of others without it being stated; - does not refer to own previous work without it being stated; - have all the references given in the literature list; - is not a copy, duplicate or copy of another's work or manuscript.	☒
3.	I/we am/are aware that violation of the above is regarded as cheating and may result in cancellation of exams and exclusion from universities and colleges in Norway, see Universitets- og høgskoleloven §§4-7 og 4-8 og Forskrift om eksamen §§ 31.	☒
4.	I/we am/are aware that all submitted theses may be checked for plagiarism.	☒
5.	I/we am/are aware that the University of Agder will deal with all cases where there is suspicion of cheating according to the university's guidelines for dealing with cases of cheating.	☒
6.	I/we have incorporated the rules and guidelines in the use of sources and references on the library's web pages.	☒

Publishing Agreement

Authorization for electronic publishing of the thesis.

Author(s) have copyrights of the thesis. This means, among other things, the exclusive right to make the work available to the general public (Åndsverkloven. §2).

All theses that fulfill the criteria will be registered and published in Brage Aura and on UiA's web pages with author's approval.

Theses that are not public or are confidential will not be published.

I hereby give the University of Agder a free right to

make the task available for electronic publishing: ☒JA ☐NEI

Is the thesis confidential? ☐JA ☒NEI

(confidential agreement must be completed and signed by the Head of the Department)

- If yes:

Can the thesis be published when the confidentiality period is over? ☐JA ☐NEI

Is the task except for public disclosure? ☐JA ☒NEI

(contains confidential information. see Offl. §13/Fvl. §13)

Table of Contents

List of Figures

List of Tables

Notation

NiF	Bare nickel foam
NiO-400-2/NiF	Nickel foam treated at 400° C for 2 hours
NiO-500-.25/NiF	Nickel foam treated at 500° C for 2 hours
NiO-500-.5/NiF	Nickel foam treated at 500° C for 2 hours
NiO-500-1/NiF	Nickel foam treated at 500° C for 2 hours
NiO-500-2/NiF	Nickel foam treated at 500° C for 2 hours
NiO-500-4/NiF	Nickel foam treated at 500° C for 2 hours
NiO-600-.5/NiF	Nickel foam treated at 600° C for 2 hours
NiO-600-1/NiF	Nickel foam treated at 600° C for 2 hours
NiO-600-2/NiF	Nickel foam treated at 600° C for 2 hours
NiO-600-4/NiF	Nickel foam treated at 600° C for 2 hours
NiO-700-2/NiF	Nickel foam treated at 700° C for 2 hours

Abbreviations

CET	Central European Time
HER	Hydrogen evolution reaction
NiF	Nickel Foam
NiO	Nickel Oxide
OER	Oxygen evolution reaction
SI	International System of Units
UiA	Universitetet i Agder

Chapter 1

Introduction

1.1 Background

Humans have employed renewable energy sources for millennia. In fact, until approximately 250 years ago, hydro, wind, solar, and biomass were the sole energy sources known and available to humans. Following the Industrial Revolution in the 18th century, human society witnessed unprecedented fossil fuel consumption to support rapid technological advancements [1]. Because of the continuous consumption of fossil fuel that has a limited reserve, it made an urgent call to find a sustainable alternative fuel for future generations. Water electrolysis offers a promising solution to produce clean hydrogen fuel [2]. Due to its high energy density of 141.9 MJ/kg and non-polluting properties, hydrogen (H_2) is receiving extensive attention for its renewable and environmentally favorable characteristics to face the ever-growing energy demand[3].

Electrocatalytic water splitting presents a potential answer to the energy crisis as a viable strategy for clean hydrogen production[4]. Electrochemical water splitting involves the breakdown of water into hydrogen and oxygen using an external electric current, facilitated by two half-cell reactions: the hydrogen evolution reaction (HER) and the oxygen evolution reaction (OER) [1]. However, the hydrogen generation by water splitting is limited due to the sluggish oxygen evolution reaction ($2H_2O \rightarrow O_2 + 4H^+ + 4e^-$), where four proton and four electron transfer is required for the formation of oxygen-oxygen bond that consumes an extra potential, higher than the theoretical value of 1.23V [5]. The necessary extra potential than theoretical potential is referred to as overpotential [6]. As the performance of water electrolysis is indicated by high overpotential, it is essential to develop an electrocatalyst that is highly active exerting low overpotential, and increases the overall process efficiency [7].

Till now, noble metal-based catalysts have shown the highest performance, such as RuO_2/IrO_2 and Platinum-based catalysts exhibit the highest activity for OER and HER, respectively [8]. However, the limited abundance on earth, high cost, and poor long-term stability of these precious metals dramatically impede their large-scale commercial applications. That's why, the development of an earth-abundant non-precious metal-based highly active, and stable electrode material is essential for the large-scale water-splitting process [9]. To date, numerous studies have been done to find non-precious metal-based active electrocatalysts with durability[10]. The recorded electrocatalysts include transition metal sulfides, phosphides, selenides, carbides for HER, and transition-metal hydroxides for OER electrocatalysts [11]. Note that HER electrocatalysts perform well in acidic electrolytes, and OER one works better under alkali conditions. The pH mismatch of the combined OER and HER electrocatalysts may unavoidably result in less effective water-splitting [11]. The developed bifunctional electrocatalysts to simplify and reduce the cost of water-splitting have shown high HER activity with relatively poor OER catalytic activity or vice versa [12], [13], [14].

For industrial applications, a non-noble bifunctional electrocatalyst is needed to be designed that can catalyze both OER and HER simultaneously [1]. Nickel foam (NiF) has been considered as a promising substrate material to produce water-splitting electrodes having high surface area, excellent conductivity, and robust mechanical properties. Traditional approaches to enhance the performance of NiF include depositing platinum group metals, transitional metal nanoparticles, sulfides, and oxides,

which have shown improved HER and OER activities [2], [15]. When catalysts are prepared in powder form and powder slurry is pasted on the conductive substrate by using a binder, there are several drawbacks. The use of binders reduces the performance by decreasing the contact area between catalytic active sites and electrolytes [16].

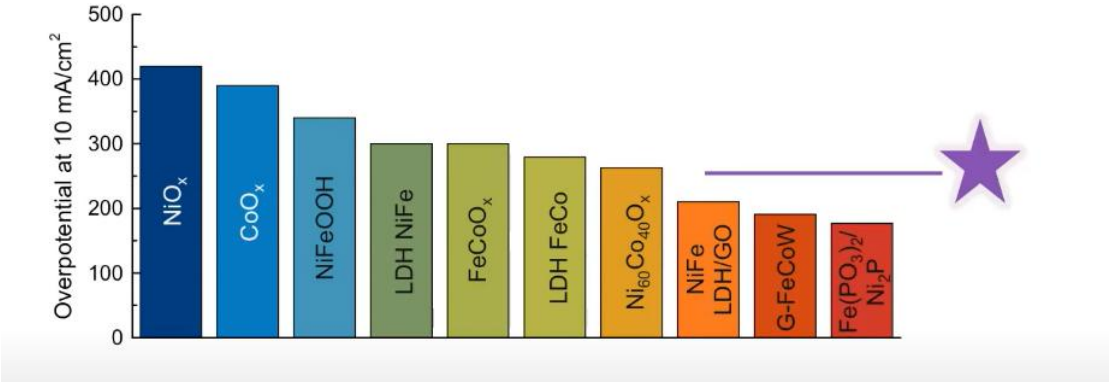

Figure 1. Catalytic activity of different electrocatalysts [17], [18], [19], [20]

To overcome this problem, a three-dimensional (3D) nickel foam substrate has gained great interest. New techniques such as acid treatments, electrochemical oxidation, sulphidation and phosphidation have further enhanced NF's catalytic activity [2], [21]. For electrode preparation acid washing is commonly used in the water electrolysis and battery technologies [22], [23]. Acid washing found to increase current density of 17.9% for HER performance of MoS2- coated nickel foam electrode [23].

Despite having advancements in electrochemical water splitting, the high cost of noble metal catalysts, additional support materials to deposit catalysts, overpotential issues, limited scalability and their stability hindered the overall progress[24]. More innovative strategies to find low-cost, non-noble electrocatalysts are urgent to overcome these challenges and advance the practical application of water-splitting[10], [25]. For the past few decades, nickel foam has gained interest as a support material to support or grow metal nanoparticles, sulfides, phosphides, oxides, and hydroxides. However, advanced simple strategies for the activation of nickel foam without the addition of additional elements as high-performing bi-functional electrodes have not been explored widely. Considering these scopes, in this thesis simple thermal modification of nickel foam strategy designed to tune the active site of nickel foam with uniform porosities as bi-functional high-performing electrode materials for electrochemical water splitting.

1.2 Aims and Objectives

This research aims to design a simple thermal treatment strategy to enhance the active sites of the nickel foam as high-performing bifunctional electrodes for electrochemical water splitting. The aim will be achieved through the objectives below,

i. Thermal treatment and optimization of the thermal treatment condition for nickel foam.
ii. Characterization of thermally treated nickel foam.
iii. Investigate the electrochemical performance of the thermally treated nickel foam for HER and OER
iv. Evaluation of full cell water splitting performance and stability of the thermally treated nickel foam.

1.3 Research Question

To guide the exploration and ensure the objectives are systematically addressed, this research is framed by the following questions:

i. What are the optimal thermal treatment conditions (e.g., temperature and duration) for enhancing the electrochemical performance of nickel foam?
ii. How does thermal treatment influence the structural, morphological, and compositional properties of nickel foam, and how do these changes improve its active sites?
iii. How does thermally treated nickel foam perform as an electrode for the HER and OER, and how do its kinetic and catalytic properties differ compared to untreated nickel foam?
iv. How efficient is thermally treated nickel foam in full-cell water splitting, and how stable is its performance over prolonged operation?

1.4 Thesis outline

This thesis contains five chapters.

Chapter 1: This chapter presents a background introduction and information about the selected problem and the objectives of this thesis followed by research questions.

Chapter 2: This chapter presents an extensive review of existing literature and theory expressing a deep insight into water splitting, electrocatalysts, their performance, advantages, and disadvantages concluding with an overview of electrocatalysts for industrial water splitting.

Chapter 3: This chapter outlines the experimental setup, methodology, material synthesis, characterization, and test procedures used for analyzing the sample.

Chapter 4: This chapter contains results and discussions that indicate the performance of modified NF analyzing the current density, overpotential, active sites, EIS, and stability.

Chapter 5: This chapter provides a concise summary of this research findings and discusses the prospective research opportunities.

Chapter 2

Theoretical Background

2.1. Water splitting

Water splitting is a fundamental electrochemical process in which water is broken down into its constituent components, hydrogen (H_2) and oxygen (O_2) . External energy is provided to carry the overall water-splitting process utilizing electrical energy or light energy (photoelectrochemical process) to overcome the binding energy [26]. Overall reaction for the water-splitting process is,

$$2H_2O\ (l) \rightarrow 2H_2\ (g) + O_2\ (g)$$

As the reaction is not spontaneous, it requires energy input to proceed. The supplied electrical energy is essential to break the bonds in water molecules. The key components of water electrolysis are electrodes, electrolytes, and power sources. As pure water has poor conductivity, the electrolyte facilitates the movement of ions in the water. NaOH or KOH is often added to water to increase the conductivity. A two-electrode or three-electrode system is used in water electrolysis, where oxidation occurs in the anode and reduction occurs in the cathode. In the anode, oxygen is produced by oxygen evolution reaction (OER) and in a cathode, hydrogen is produced by hydrogen evolution reaction (HER).

At the cathode, as reduction occurs, the water molecules obtain electrons and are reduced to hydrogen gas,

In an Acidic aqueous solution,

$$\mathbf{2H^+ + 2e^- \rightarrow H_2}$$

In an alkaline aqueous solution,

$$\mathbf{2H_2O + 2e^- \rightarrow H_2 + 2OH^-}$$

At the anode, as oxidation occurs, oxygen gas and protons is produced,

In an acidic aqueous solution,

$$\mathbf{2H_2O \rightarrow O_2 + 4H^+ + 4e^-}$$

In an alkaline aqueous solution,

$$\mathbf{4OH^- \rightarrow O_2 + 4e^- + 2H_2O}$$

The minimum energy required to electrolyze water is determined by the Gibbs free energy of the reaction. The theoretical thermodynamic potential needed to split water is 1.23V [27]. Due to the electrode's overpotential and resistance, extra energy is necessary to proceed with the reaction, the actual potential required is higher than the theoretical potential. This extra potential needed is called overpotential. Even with high overpotential, the OER and HER follow the Butler-Volmer reaction model [12].

2.2. Hydrogen

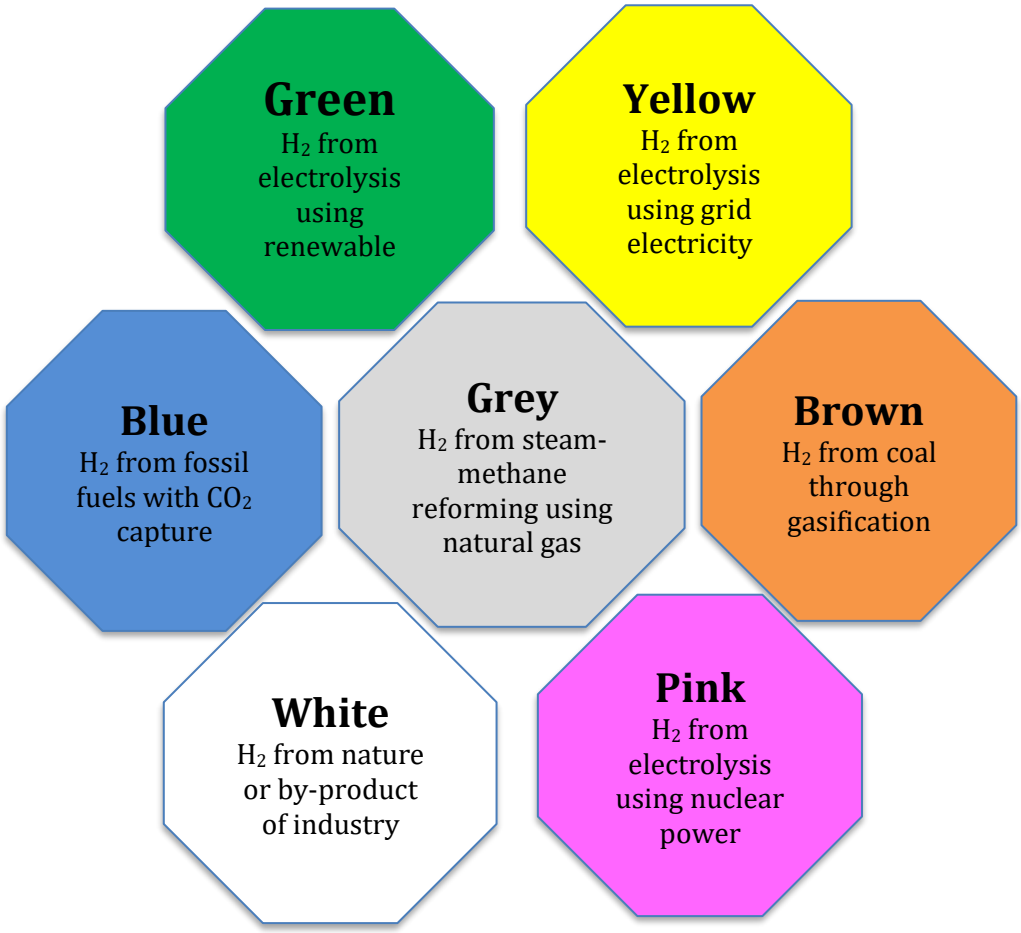

Figure 2. 1 The different colors are employed for hydrogen to indicate their origin and environmental impact [22].

In 2024, global hydrogen production reached approximately 100 million tons (Mt), which represents a continuous annual growth trend over the past decade. For the last ten years, the recorded average hydrogen production per year is 95 Mt for industrial applications. Refining processes and ammonia production for fertilizers dominate the traditional uses of hydrogen. However, emerging applications in heavy industry, long-haul transportation, and energy storage. Since the application of hydrogen as energy storage is at an early stage of development, representing less than 1% of total demand despite significant growth in low-carbon hydrogen production in recent years. Currently, molecular hydrogen is mainly produced in the chemical industry by the steam reforming of natural gas.

Hydrogen is pivotal in renewable energy systems as a versatile energy carrier and storage medium[28]. It provides solutions for balancing intermittent renewable energy sources, such as solar and wind, by storing surplus energy in the form of hydrogen through electrolysis. This stored energy can be reconverted to electricity or used in industrial processes. Moreover, green hydrogen, produced entirely from renewable energy, has emerged as a critical component in decarbonizing sectors like steelmaking and shipping, which are difficult to electrify .

2.3. Electrochemical cell

2.3.1 Three-electrode system

The three-electrode system is a fundamental and widely employed configuration for studying electrochemical processes, including water electrolysis. This electrode system provides precise control and measurement of the electrochemical behavior of individual electrodes, making it indispensable for characterizing the hydrogen evolution reaction (HER) and oxygen evolution reaction (OER) involved in water splitting.

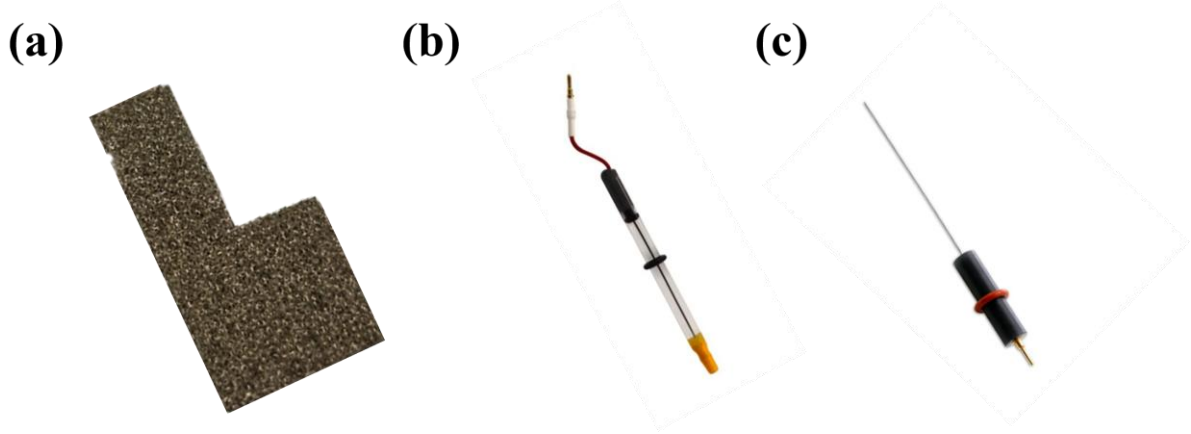

Figure 2. 2 (a) Working electrode (b) Reference electrode [23] (c) Counter electrode[24].

In a three-electrode setup for water electrolysis, the working electrode (WE) serves as the site of the electrochemical reaction under investigation. Materials for the working electrode are chosen based on their catalytic activity, conductivity, and stability, such as platinum, nickel, or advanced transition metal-based electrocatalysts.

The counter electrode (CE), often made of an inert material like platinum or graphite, completes the electrical circuit by providing a surface for the counter-reaction. For instance, if the HER is being studied at the working electrode, the counter electrode facilitates the OER, ensuring the current flow between the two electrodes. The counter electrode is designed to have sufficient size and stability to handle the current densities involved in the process without affecting the accuracy of measurements.

The reference electrode (RE) is a critical component that allows precise measurement of the working electrode's potential relative to a stable and known reference point. Commonly used reference electrodes for experiments are the saturated calomel electrode (SCE) or silver/silver chloride electrode (Ag/AgCl). The reference electrode does not participate in the electrochemical reactions, like the counter electrode, but provides a constant potential to accurately measure the working electrode's voltage. This decoupling of potential measurement from current flow is a key advantage of the three-electrode system over a two-electrode system.

To perform a detailed investigation of the catalytic properties of electrode materials, a three-electrode system is widely used to evaluate the critical parameters such as overpotential, Tafel slopes, and exchange current densities, which are essential for understanding and optimizing HER and OER kinetics. Additionally, using the system provides insight into reaction mechanisms, stability, and the impact of electrolyte composition and pH on performance.

To develop efficient electrocatalysts, the three-electrode system is considered an essential tool for research in water-splitting technologies. Isolating the behavior of the working electrode ensures accurate and reproducible measurements, paving the way for improved energy conversion processes.

A three-electrode system is used in this study where oxidized NiF is used as the working electrode, a platinum (Pt) electrode is used as the counter electrode, and an Ag/AgCl (3M KCL) electrode is used as the reference electrode.

2.3.2 Two-electrode system

A two-electrode system is a simple electrochemical configuration used to study the performance of electrochemical reactions and devices. It consists of an anode and a cathode, both immersed in an electrolyte. The working electrode is the site of the primary electrochemical reaction under investigation, while the counter electrode completes the circuit and facilitates the current flow.
In this system, the potential difference is applied or measured between the two electrodes, and the resulting current reflects the electrochemical activity. However, since the system does not include a reference electrode, the potential of the working electrode is not independently controlled but is measured relative to the counter electrode. The simplicity of two-electrode setup makes it suitable for applications like energy storage devices, such as batteries and capacitors, where the focus is on overall device performance rather than detailed mechanistic studies. However, its limitation lies in the inability to decouple the contributions of individual electrodes, which can be addressed using a three-electrode system for more detailed investigations.

2.4. Electrocatalyst

Electrocatalysts referred to the materials that can enhance and accelerate electrochemical reactions. Electrocatalyst plays an important role in energy conversion and storage technologies, increasing the efficiency and kinetics of critical reactions, such as the HER, OER, and ORR. Electrocatalysts consist of metals, metal oxides, or metal alloys, with noble metals such as platinum and iridium.
The efficiency of an electrocatalyst depends on evaluation according to factors including activity, stability, selectivity, and durability under operational settings. Improvements in electrocatalyst design are essential for the advancement of sustainable energy technologies since they directly affect the efficiency and viability of devices used in applications like water splitting, CO_2 reduction, and renewable energy storage.

2.5. Electrolyte

In electrochemistry, the electrolyte is the substance that conducts the electricity through the movement of ions when dissolved in a solvent. Electrolytes are typically salts, acids, or bases that dissociate into positively charged cations and negatively charged anions when dissolved in a solvent, usually in water. 1M KOH solution is used as the electrolyte in this study to prepare the three-electrode system. 6M KOH solution is used as electrolyte to investigate the full cell stability in a two-electrode system.

2.6. Nickel foam

Nickel foam is a porous metal with a unique sponge-like structure. It offers 95% or higher porosity and a high surface area to volume ratio. Its excellent electrical conductivity and chemical stability make it suitable for catalysis, energy storage, filtration and heat exchanger. Its high porosity makes it efficient for electron transfer and mass transfer, which properties are essential to produce batteries, supercapacitors, fuel cells and electrolyser. Nickel foam is manufactured using various techniques to

obtain desired structural properties and pore size including electroplating and chemical vapor deposition.

Electrochemical test

2.7. Linnear Sweep Voltammetry

Linear sweep voltammetry (LSV) is a widely used electrochemical technique that involves sweeping the working electrode's potential linearly with time relative to a stable reference electrode while recording the resulting current. In a three-electrode system, the working electrode is where the reaction of interest occurs, the reference electrode provides a stable potential for accurate measurements, and the counter electrode facilitates current flow. For water electrolysis, LSV is used to investigate the HER at the cathode and OER at the anode. During LSV, the potential is swept within a defined range while the corresponding current is recorded, generating a current-potential curve. Critical data obtained from LSV include the onset potential, which indicates the potential at which the reaction initiates, the overpotential required to drive the reaction, and the current density, which reflects the electrocatalytic activity. This data is analyzed to determine critical performance metrics such as Tafel slopes, exchange current densities, and overall catalytic efficiency. For HER and OER, LSV data can reveal the effectiveness of a catalyst in reducing energy barriers, as lower overpotentials and higher current densities indicate superior catalytic performance. Additionally, it provides insights into the stability and kinetics of the catalyst, aiding in the evaluation and optimization of materials for efficient water-splitting technologies. The polarization curves were recorded by linear sweep voltammetry (LSV), and the potentials were converted to a reversible hydrogen electrode (RHE) according to the Nernst equation,

$$E_{RHE} = E_{Hg/Hgo} + 0.059 \times pH + E^{o}{}_{Hg/HgO} \quad (2)$$

where $E_{Hg/HgO}$ is the measured potential against the reference electrode and $E^{o}{}_{Hg/HgO}$ equals 0.098 at standard room temperature and pressure[29].

2.8. Chronopotentiometry

Chronopotentiometry (CP) is an electrochemical technique in which a constant current is applied to the working electrode in a three-electrode system, and the resulting potential is measured as a function of time. In this configuration, the reference electrode ensures accurate potential measurement, while the counter electrode facilitates current flow to complete the circuit. For water electrolysis, CP is employed to study the stability and catalytic activity of materials for the hydrogen evolution reaction (HER) and oxygen evolution reaction (OER). During the experiment, a steady current density is applied, mimicking operational conditions, and the working electrode's potential response is recorded over time. The obtained data provides measure of the overpotential required to sustain the reaction and any variations in potential, which may indicate changes in catalytic activity or degradation of the electrode material. Analysis of this data involves monitoring the stability of the overpotential, with a constant potential indicating stable performance and deviations suggesting catalyst degradation or passivation. For HER and OER, CP data provides insights into the durability and efficiency of electrocatalysts, with lower and more stable overpotentials reflecting superior catalytic

activity and robustness under prolonged operation. Thus, CP is a crucial technique for evaluating the long-term viability of electrocatalysts in water-splitting applications.

2.9. Electrical Impedence Spectroscopy

Electrical impedance spectroscopy is a technique for examining the electrical characteristics of materials and interfaces. The electrical impedance is measured across a range of frequencies to investigate charge transfer, ion diffusion, and capacitive phenomena. EIS characterizes these processes by analyzing the system's response to an alternating current (AC) signal, allowing it to determine and compare resistive, capacitive, and inductive behavior within the studied system. Data are typically present in the form of Nyquist or Bode plots, from which parameters such as charge transfer resistance and double-layer capacitance can be derived.

EIS is widely employed in electrochemistry to study electrode-electrolyte interfaces, corrosion mechanisms, and battery systems. Its ability to decouple multiple concurrent processes makes it ideal for analyzing electrochemical kinetics and diffusion phenomena. In water electrolysis, EIS is used to evaluate the performance of catalysts, assess electrolyte properties, and optimize cell designs. Analyzing the impedance spectra, the measure of losses due to ohmic resistance, charge transfer at the electrodes, and mass transport limitations provides insights into improving hydrogen production efficiency.

EIS calculations often involve fitting experimental impedance data to equivalent circuit models that represent the physical and chemical processes within the electrochemical system. Commonly used components include resistors, capacitors, and constant phase elements (CPEs), which approximate non-ideal capacitive behavior. Mathematical techniques such as complex nonlinear least squares (CNLS) fitting are used to extract parameters from the impedance spectra, which enable quantitative analysis of the system's characteristics.

2.10. Onset potential

The onset potential in a three-electrode system is the specific potential at which a measurable current begins to flow, signaling the initiation of an electrochemical reaction at the working electrode. For water electrolysis, the onset potential represents the voltage at which the hydrogen evolution reaction (HER) or oxygen evolution reaction (OER) starts to occur. To determine the onset potential, linear sweep voltammetry (LSV) is typically employed, where the potential of the working electrode is swept while the current response is recorded. The onset potential is identified as the point on the current-potential curve where a significant deviation from the baseline current is observed. This data is analyzed by extrapolating the linear portion of the current response to intersect with the baseline, providing a precise value for the onset potential. A lower onset potential for HER or OER indicates a catalyst's ability to initiate the reaction with minimal energy input, reflecting high catalytic activity. Additionally, the onset potential provides insights into the kinetics and efficiency of the electrocatalyst, as well as its potential to reduce energy losses in water-splitting applications. Evaluating onset potential is therefore critical in assessing and optimizing materials for sustainable hydrogen production. The onset potential is often considered a simple parameter used to determine a material's relative activity.

2.11. Overpotential

Overpotential is a critical factor influencing the efficiency of water electrolysis, particularly in the hydrogen evolution reaction (HER) and oxygen evolution reaction (OER). In water electrolysis, overpotential refers to the extra potential required, beyond the thermodynamic equilibrium potential, to drive the HER and OER at a measurable rate. It arises from kinetic barriers such as charge transfer, mass transport, and activation energy associated with these reactions.

For the HER, which occurs at the cathode, overpotential is primarily influenced by the slow kinetics of proton reduction and hydrogen atom recombination on the electrode surface. The OER, occurring at the anode, typically requires a much higher overpotential due to its inherently sluggish kinetics, involving the transfer of four electrons and the formation of oxygen-oxygen bonds. The OER is generally considered the rate-limiting step in water electrolysis because of its complex reaction mechanism and higher activation energy.

It is a crucial challenge to minimizie the overpotential for improving water electrolysis systems' energy efficiency. It is typically achieved through high-activity and stability electrocatalysts, tailored electrode materials, and optimized operating conditions. By reducing the overpotential for both HER and OER, the overall energy consumption of water splitting can be significantly reduced, making it a more viable method for sustainable hydrogen production.

2.12. Tafel equation

The Tafel equationin electrochemical kinetics describes the dependence of the overpotential (η) on the logarithm of the current density (j) for an electrode reaction. It is expressed mathematically as,

$$\eta = a + b \log(j) \quad (1)$$

where a is the intercept, b is the Tafel slope, and j represents the current density. The Tafel slope (b) is a critical parameter that provides insights into the reaction mechanism and the rate-determining step. Derived from the Butler-Volmer equation under conditions of high overpotential, the Tafel equation is particularly useful for analyzing and comparing the performance of electrocatalysts in processes such as hydrogen evolution, oxygen reduction, and other redox reactions. Its application enables researchers to evaluate the efficiency and kinetics of electrode materials in various electrochemical systems.

For, HER Tafel Slopes,

i. 120 mV/dec: Volmer reaction(discharge step).
ii. 40 mV/dec: Heyrovsky reaction(electrochemical desorption).
iii. 30 mV/dec: Tafel reaction(recombination of adsorbed hydrogen).

For OER Tafel Slopes,

i. 120 mV/dec or higher: Indicates sluggish kinetics (rate-limiting step likely involves multiple electron transfers).
ii. 60-90 mV/dec: Suggests faster kinetics and more efficient OER catalysts.

2.13. Nyquist plot

A Nyquist plot is a graphical tool commonly used in electrochemical impedance spectroscopy (EIS) to analyze the impedance of an electrochemical system. It plots the imaginary part of impedance (Z2) on the y-axis against and the output impedance (Z1) on the x-axis, creating a curve that often takes the shape of a semicircle or a series of arcs. Frequency is not explicitly shown on the axes but is represented along the curve, starting from high frequency and decreasing to low frequency. In electrochemistry, the Nyquist plot is often used in the scientific community to study reaction kinetics, evaluate double-layer capacitance, and model equivalent circuits that simulate the physical processes, such as resistance, capacitance, and diffusion, within the system. It is useful in the assessment of the performance of materials in applications of batteries, fuel cells, catalysts, and supercapacitors. The results of a Nyquist plot provide significant insights: the diameter of the semicircle corresponds to the charge transfer resistance (R_{ct}), with a smaller diameter indicating lower resistance and faster reaction kinetics. The x-axis intercept at high frequencies reveals the solution resistance (Rs), which reflects the electrolyte's conductivity. A linear portion appears in the Nyquist plot due to the mass transportation and diffusion-controlled processes at low frequencies. The deviations from the ideal semicircle indicate other factors, including adsorption effects, surface roughness, or inductive behavior. Here, the Nyquist plot is used as an analytical tool to investigate the charge transfer resistance for OER and HER in a three-electrode electrochemical setup.

Chapter 3

Methodology

3.1 Flowchart of the experiment

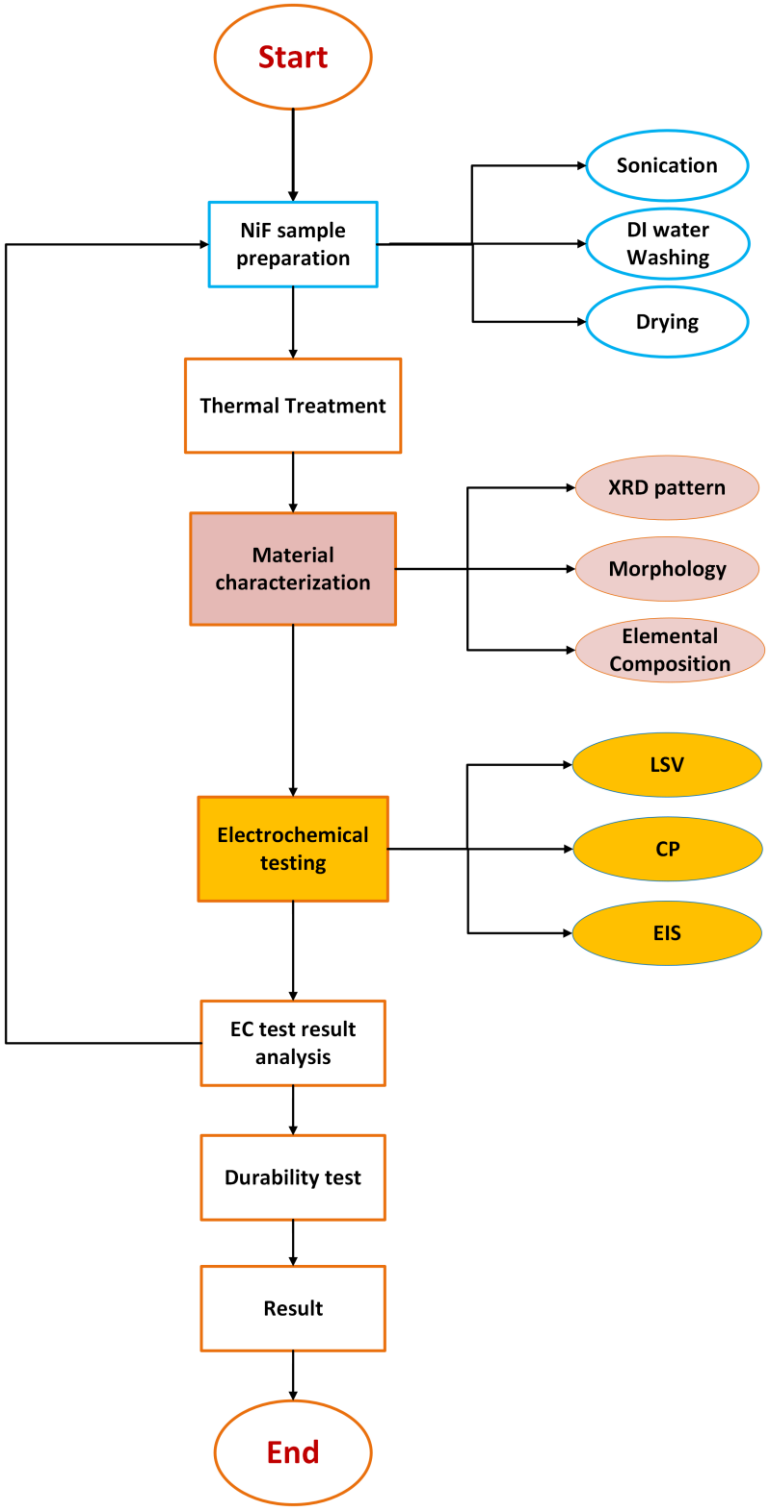

Figure 3. 1 Flowchart of the experiment

3.2 NiF sample preparation

99.8% pure porous nickel foam was purchased from Sunshinelantian, China. Its thickness is 1.5mm, porosity is (95-97)%, through hole rate is 95% and pore diameter is (0.2-0.6) mm. The porous and open structure of NiF in Fig 3.2 allows it to hold element as a substrate and facilitate reactant for better access into the three dimensional interior surface.

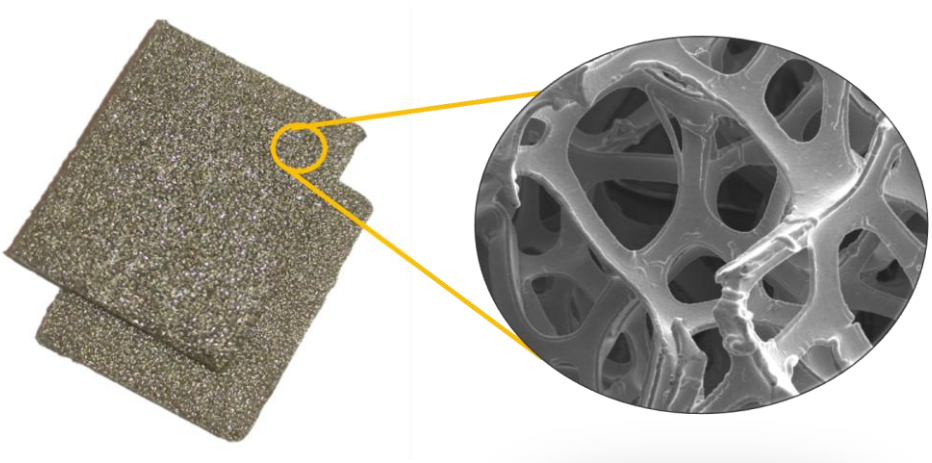

Figure 3. 2 Commercially available Nickel Foam sheet

After preparing the sample electrode to the required size (1 cm^2), it was ultrasonically cleaned for 5 minutes using a ultrasonic cleaner (IRONSIDE, USA). Then, it was rinsed with deionized water to eliminate the surface contaminants and dried in air at ambient temperature. To avoid any further contamination, a cleaned beaker and tweezers were used.

3.3 Thermal treatment of NiF for the synthesis of NiO/NiF

Clean NiF sample was synthesized by direct thermal annealing in a muffle furnace (Nabertherm P330, Germany) at the heating rate 5° C/min in an air atmosphere. To avoid contaminatin in furnace, it is cleaned throughly and clean crucible is used. After thermal treatment each sample is allowed to be cooled in ambient temperature before collection. Electrode samples treated in different temperature and duration as table below.

Table 1 : Description of sample name, thermal treatment temperature and duration

Sample Number	**Sample name**	**Thermal treatment temperature** (° C)	**Duration** (Hours)
1	NiF	-	-
2	NiO-400-2/NiF	400	2
3	NiO-500-2/NiF	500	2
4	NiO-600-2/NiF	600	2
5	NiO-700-2/NiF	700	2

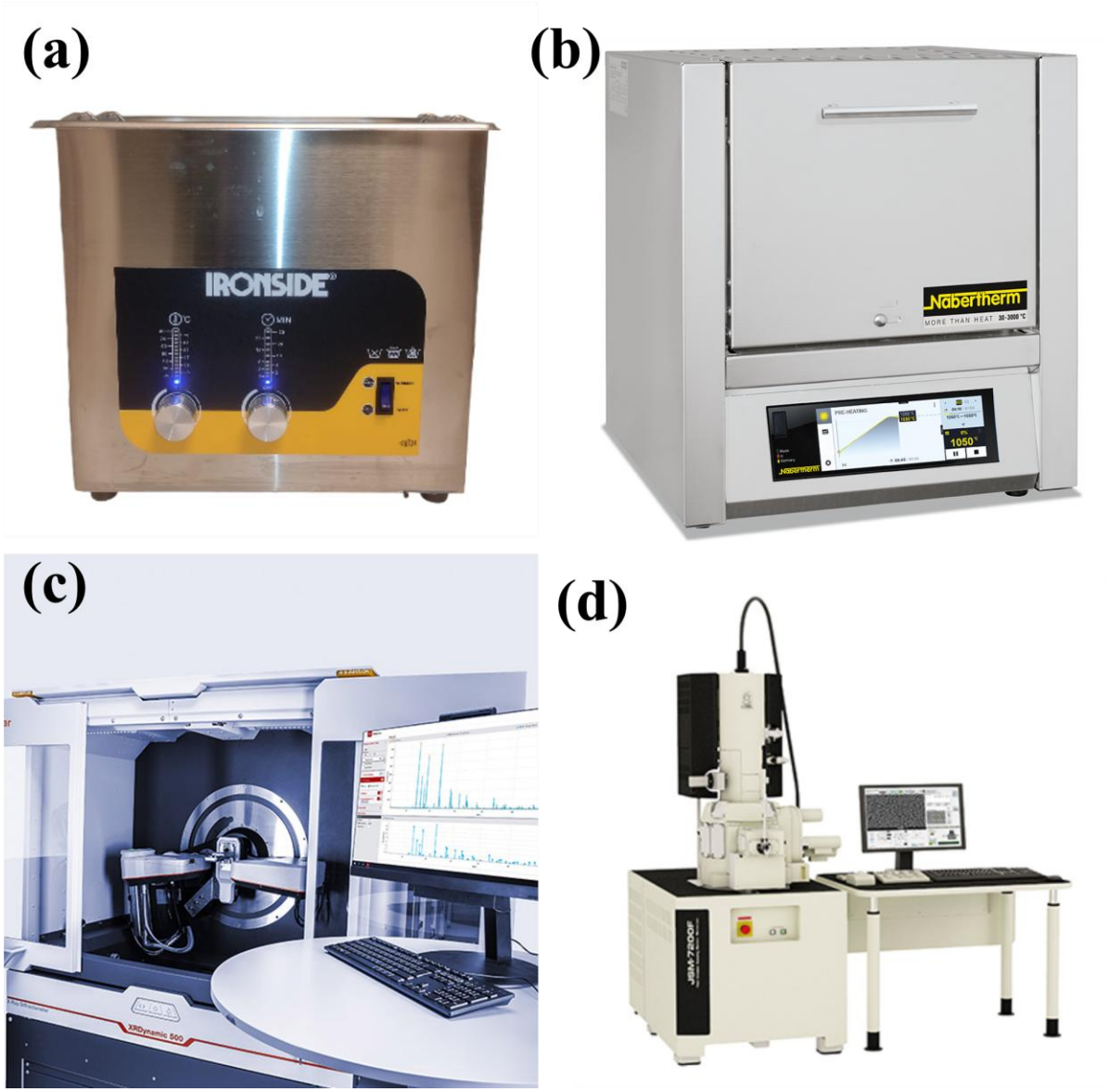

Figure 3. 3 (a) Ultrasonic cleaner (b) Muffle furnace[26] (c) X-ray Diffractometer (XRD)[27] (d) Field emission scanning electron microscope[28]

3.4 Material characterization

3.4.1 X-ray Diffraction pattern analysis

To investigate the crystal structural properties of thermally modified NiF, a X-ray diffractometer (XRDynamic 500, Anton Paar) is used. It is an analytical tool to study phase and crystallographic structure of materials.

3.4.2 Morphology and elemental composition analysis

A Field Emission – Scanning Electron Microscope (FE-SEM, JEOL JSM-7200F, Japan) is used for morphological and structural characterization. It is a type of advanced electron microscope equipped with a field emission source to produce high-resolution image of a sample. It uses field emission gun which emits electron from a sharp tip under a strong electric field. This results a narrow electron beam reducing samle damage. This technology provides high resolution image capturing capabilities with detailed topographical and elemental information about the sample. The SEM was equipped with a back-scattered electron (BSE) detector for imaging and energy-dispersive X-ray spectroscopy (EDS) for compositional analysis. The SEM was operated at 15 kV during obtaining images and EDS results. To investigate the elemental composition EDS images is analyzed for thermally modified NiF sample.

3.5 Experimental methods

3.5.1 1M KOH Electrolyte preparation

1M potassium hydroxide (KOH) electrolyte was prepared from KOH flakes with precision and safety. First, 56.1 grams of KOH flakes were accurately weighed using a calibrated balance, as this amount corresponds to the molar mass of KOH for 1 liter of a 1M solution. Since KOH is highly active base and corrosive, all safety precautions were taken, including wearing gloves and goggles. The weighed flakes were then slowly added to approximately 800 mL of distilled water in a heat-resistant beaker. During the process, the solution became warm due to the exothermic nature of the reaction. The mixture was stirred gently with a non-reactive stirrer to ensure the complete dissolution of the flakes. Once the solution had cooled to room temperature, it was transferred into a 1-liter volumetric flask. More distilled water was added to the solution gradually until the total volume reached 1 liter. The solution was then mixed thoroughly to ensure uniformity and stored in a sealed, labeled container to prevent contamination or absorption of carbon dioxide from the air.

3.5.2 6M KOH Electrolyte preparation

To prepare a 6M KOH electrolyte solution, 336.6 grams of KOH flakes were taken and mixed with distilled water following the same procedure described at (3.4.1). All safety measure were taken during solution preparetion and handling.

3.5.3 Experimental setup

A three-electrode setup is employed consisting of thermally modified nickel foam as working electrode, platinum wire as counter electrode with Ag/AgCl reference electrode and 1.0M KOH solution as electrolyte as shown in figure. Using a small-scale setup eliminated the distance between the three electrodes and allows a high degree of reproducibility.

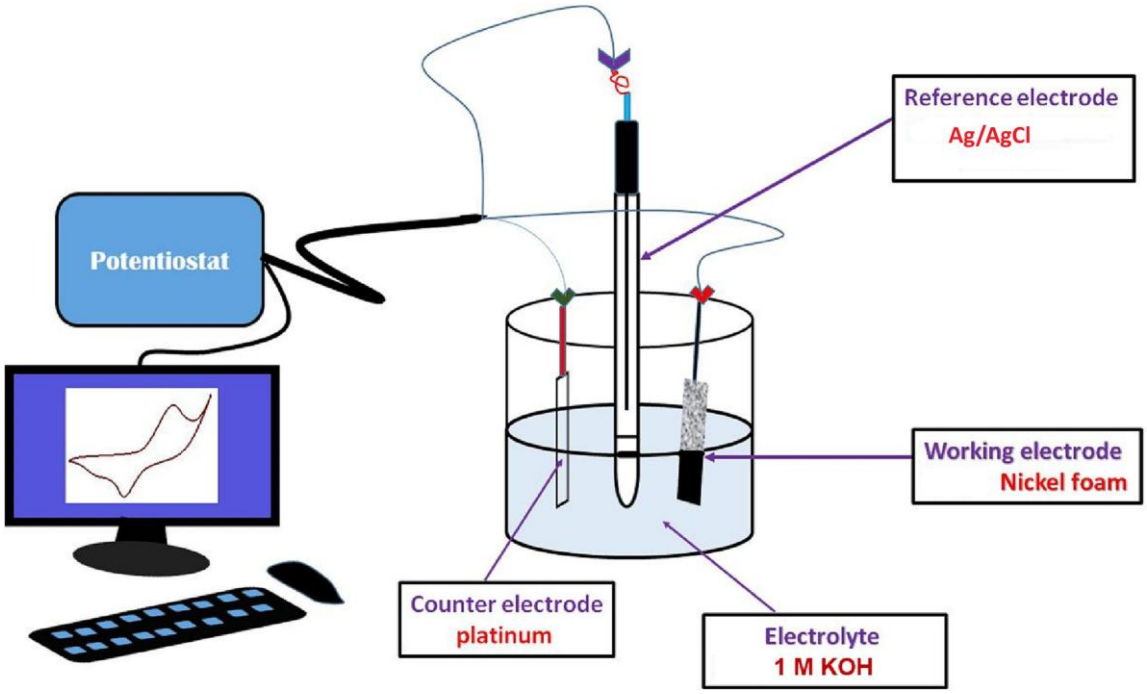

Figure 3. 4 Experimental setup of electrochemical test [21].

Using a potentiometer (IVIUMSTAT), linnear sweep voltametry (LSV) was performed at the range of 0 to 2.0 V for OER and from -0.9 to -3.0 V_{RHE} fro HER with a sweep rate of 5 mV s^{-1}. Open circuit electrochemical impedance spectroscopy (EIS) was measured at frequiencies from 1×10^5 to 0.1 Hz with a sinusoidal amplitude of 5mV and 10 points per decade. Chronopotentiometry (CP) was measured at the current density of 100 $mAcm^{-2}$ for OER and at -100 $mAcm^{-2}$ for HER.

Chapter 4

Results and Discussion

4.1 XRD Analysis of thermally modified NiF at different temperature

The phase constitution and crystalline structures of thermally treated NiF were studied using XRD. Fig 4.1 (a-c) shows the XRD pattern of NiF before and after thermal treatment at different temperatures ranging from 400 to 700° C.

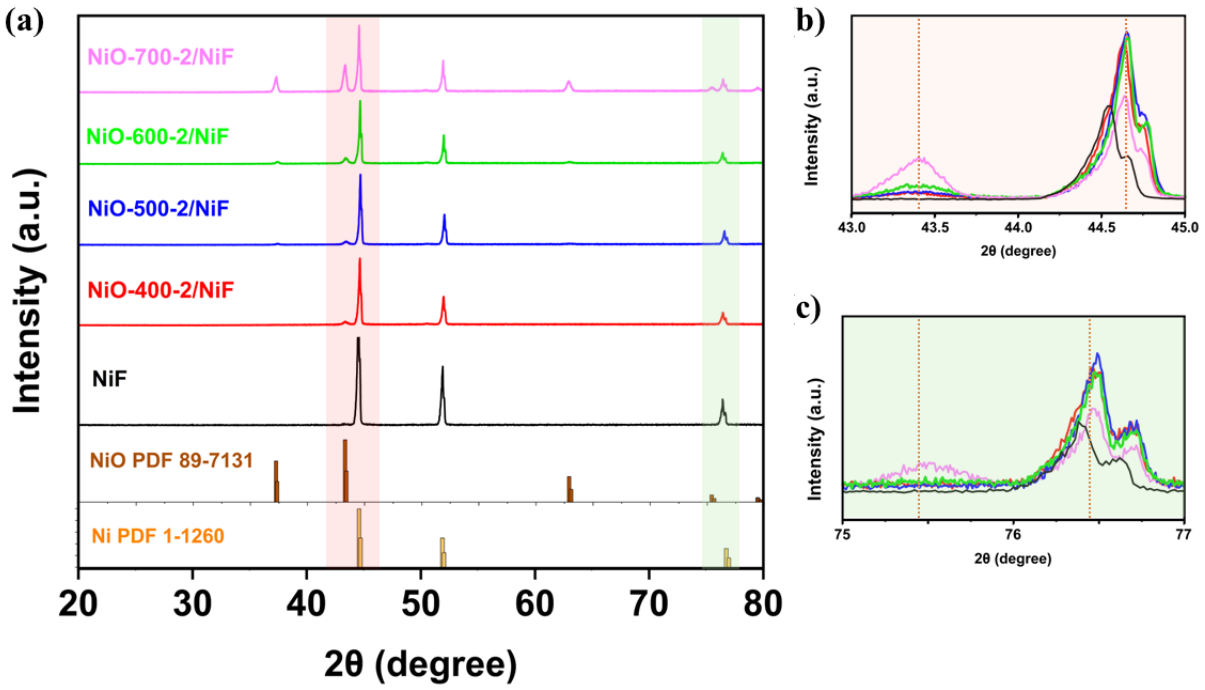

Figure 4. 1 (a). XRD pattern of nickel oxide (NiO) on NF substrate after oxidation at different temperatures.(b) Overlapped peaks of (43-45) 2Θ degree. (c) Overlapped peaks of (75-77) 2Θ degree.

The XRD pattern of bare nickel foam exhibits diffraction peaks at 2θ angles of 44.5°, 51.8°, and 76.4°, corresponding to the (111), (200), and (220) planes, respectively, of metallic nickel (Ni) with a face-centered cubic (FCC) structure. observed peaks match JCPDS card 1-1260, a standard reference for pure nickel. The peak at the plane (111) exhibits the highest intensity, which indicates that this crystallographic plane is the most predominant in the metallic nickel lattice. Peaks at the relatively lower intensities (200) and (220) also correspond well with the intensity of the JCPDS 1-1260 card. These peak's sharpness and well-defined nature suggest that the nickel foam is highly crystalline. As no other peaks are found corresponding to nickel oxides or other phases, this indicates that the nickel foam is in its metallic state and is largely unoxidized. This establishes a baseline for understanding and comparing oxidation effects on NiF crystal structure and surface properties.

The XRD patterns of nickel foam samples (NiO-400-2/NiF, NiO-500-2/NiF, NiO-600-2/NiF, and NiO-700-2/NiF) exhibit significant differences compared to the bare NiF, with additional peaks corresponding to the cubic phase of nickel oxide (NiO). These peaks, which appear at 2θ angle = 37.2°, 43.3°, 62.9°, 75.4° and 79.4°, are assigned to the (111), (200), (220), (311), and (222) planes of NiO, respectively, based on the reference data in JCPDS card 89-7131. The intensity of these NiO peaks increases

progressively with the oxidation temperature (same duration), indicating enhanced oxidation and crystallization of the nickel foam surface.

For NiO-400-2/NiF, the XRD pattern shows the initial formation of NiO, as evidenced by the weak peaks at 37.2°, 43.3°, and 62.9° angles in Fig.4.1(a). However, the nickel peaks at 44.5°, 51.8°, and 76.4° remain dominant, suggesting low oxidation at this temperature. According to the SEM image in Fig,4.2 (c-e), the thin and uneven oxide layer formed at 400°C-2 hour also supports the obtained NiO peaks in XRD. The Ni peaks of this (NiO-400-2/NiF) sample do not suppress the nickel peaks of untreated nickel samples, which retain much of their original intensity.

The XRD pattern of NiO-500-2/NiF exhibits more visible NiO peaks, particularly for the (111) and (200) planes at 37.2° and 43.3° respectively, corrresponding to JCPDS 89-7131, indicating the formation of a thicker and well-crystallized NiO layer. At the same time, the metallic nickel peaks are reduced in intensity compared to the bare NiF and NiO-400-2/NiF samples, suggesting that a significant portion of the nickel surface is oxidized. This sample exhibits a balance between oxidation and metallic nickel, containing in a well-defined NiO layer and porous NiF surface that increased conductive surface area.

In NiO-600-2/NiF, the NiO peaks become even more intense, while the metallic nickel peaks are significantly diminished. This indicates the formation of a high amount of NiO on NiF surface. The dominance of the NiO peaks for the (111), (200), and (220) planes at 37.2°, 43.3°, and 62.9° 2Θ angles (JCPDS 89-7131) in Fig.4.1 (a) & (b) indicates that oxidation has progressed extensively, leaving minimum exposed metallic nickel on the NiF surface. At 2Θ angle of 76.4° in Fig.4.1(c), peak shift is observed for NiO-600-2/NiF sample that suggests formation of NiO . This obtained thick oxide layer enhances the catalytic properties by providing more active sites but also slightly reduce electrical conductivity covering the porous holes.

The XRD pattern of NiO-700-2/NiF exhibits the intense NiO peaks for the (111), (200), (220),(311),(222) planes at 2θ angle = 37.2°, 43.3°, 62.9°, 75.4° and 79.4° respectively in Fig4.1(a). It indicates the formation of a high amount crystalline and thick NiO layer. Significant peak shift is observed for this sample in Fig.4.1(b) and (c) that suggest of formation new composition of NiO on NiF surface. The metallic nickel peaks are reduced and NiO peaks are increased in intensity, that hints high amount of oxidation of the nickel foam surface. Though the active site is increased due to the extensive oxidation , it covers the surface reducing porosity that lowers conductivity, potentially affecting the electrode's electrochemical performance.

4.2 Morphology analysis of thermally modified NiF at different temperature

The morphologies of NiO/NF after oxidation at different temperatures were investigated at different magnification using a Field Emission Scanning Electron Microscope. Fig.4.2 shows the SEM images of electrodes before and after thermal treatment. In the low- and high-magnification images Fig.4.2(a-b) of bare nickel foam, it exhibits a smooth and well-defined macropores, as seen. The surface of the nickel foam appears relatively clean and unmodified, with no significant microstructural or nano structural features, reflecting the pristine state before thermal treatment. The sample oxidized at 400°C for 2 hours (NiO-400-2/NiF) demonstrates a slight roughening of the nickel foam surface, as seen in Fig.4.2(d). Higher magnification images Fig.4.2(e) reveal the formation of a thin oxide layer with grain-like structures. These features suggest the initial formation of NiO with limited crystallinity surface coverage, likely resulting in moderate enhancement of the surface area compared to the bare nickel foam. The surface became coarse and rougher than before which increases the active sites for reactant molecules. Rough surface on

nickel foam enhances performance of electrochemical reaction by increasing electron transfer and reducing gas bubble adhesion on the surface.

At 500°C (NiO-500-2/NiF), the NiO layer becomes more prominent, as evidenced by the rougher surface and more distinct microstructural features in Fig.4.2(f). The oxide grains appear larger and more densely packed, indicating improved crystallinity and oxide growth. The NiO layer observed in image Fig.4.2(g-h) suggests increased active surface sites, which can positively influence the electrocatalytic activity for water-splitting reactions such as the HER and OER.

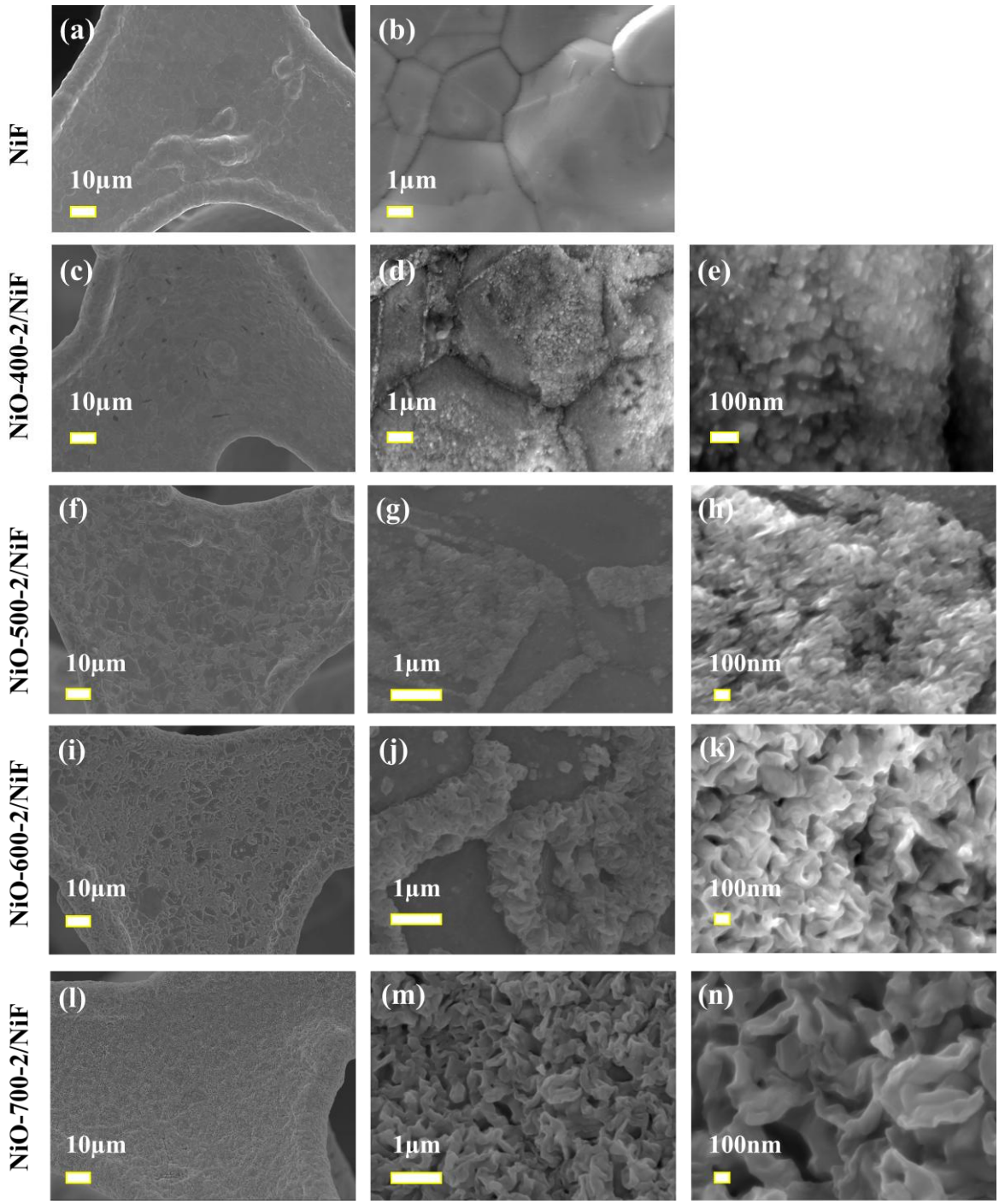

Figure 4. 2 FE-SEM images of NiO/NiF films oxidized at different thermal condition (a-b) Bare Nickel Foam (c-e) NiO-400-2/NiF (f-h) NiO-500-2/NiF (i-k) NiO-600-2/NiF (l-n) NiO-700-2/NiF

A significant morphological transformation results from the thermal oxidation of the sample (NiO-600-2/NiF) at 600°C for two hours. The NiO layer develops a highly textured surface with clearly visible interconnected structures Fig.4.2(i). At higher magnification images Fig.4.2(j-k), the formation of nanostructured nanosheets and nano-petals features is observed. This significant increase of nickel oxide microstructures contributes to excess specific surface area and enhances the electrode material's activity towards electrochemical reactions. The uniformity and hierarchical nature of rough nanostructure indicate better oxidation conditions for generating a high-density active surface.
The sample treated at 700°C (NiO-600-2/NiF) shows further structural changes, with a denser and more rugged oxide layer Fig.4.2(l). However, at higher magnifications Fig.4.2(m-n), the surface appears coarser and potentially more compact, suggesting excessive oxidation. This overgrowth may reduce the effective active surface area due to the agglomeration of oxide grains. Additionally, excessive thermal treatment could introduce mechanical stresses or defects and reduce porosity, which compromises the stability and activity of the electrode material for HER and OER.

4.3 Elemental composition analysis of thermally modified NiF at different temperature

The EDS maps of bare nickel foam Fig 4.3 (a-d) show a predominance of metallic Ni with minimal oxygen presence, elemental composition image is indicating the absence of significant oxidation. The lack of NiO coverage leads to poor catalytic activity for both HER and OER, as metallic Ni is less effective in providing active sites for water-splitting reactions. The uniform metallic surface ensures high electrical conductivity but lacks the essential chemical reactivity provided by oxides. The absence of significant contaminant indicates the high purity of the material. Such features make nickel foam suitable for electrocatalytic applications, where surface oxidation can enhance activity in oxygen evolution (OER) and hydrogen evolution reactions (HER).
The EDS maps of NiO-400-2/NiF Fig.4.3(e-h) demonstrate the formation of a thin layer of nickel oxide (NiO) distributed over the foam surface. Oxygen is detected in greater amounts compared to the bare foam, but the proportion of NiO remains relatively low. This composition refers to slight decrease of Ni amount due to partial oxidation. This reflects the formation of a thin NiO layer while retaining a significant metallic Ni core. The incomplete oxidation limits the availability of catalytically active sites, potentially leading to low performance for HER and OER. While the presence of NiO enhances the chemical activity, the limited oxide coverage restricts the potential catalytic performance.
NiO-500-2/NiF demonstrates a well-proportioned distribution of Ni and O in Fig.4.3(i-l) of the EDS analysis. The formation of a moderately thick and uniformly distributed NiO layer, while preserving a substantial amount of metallic Ni and maintaining porosity, creates an ideal environment for efficient HER. The activity of electrode is enhanced for the increase of NiO layer which enables the adsorption and mass transfer in the reaction. Additionally, increased porosity of metallic Ni ensures superior electrical conductivity, enabling effective charge transfer during the reaction. The increased ratio of oxygen content indicates an adequately oxidized surface, which increases the number of active sites without compromising conductivity. This precise balance between the oxidized NiO layer and the porosity of Ni foam surface is a key factor in optimizing HER performance.

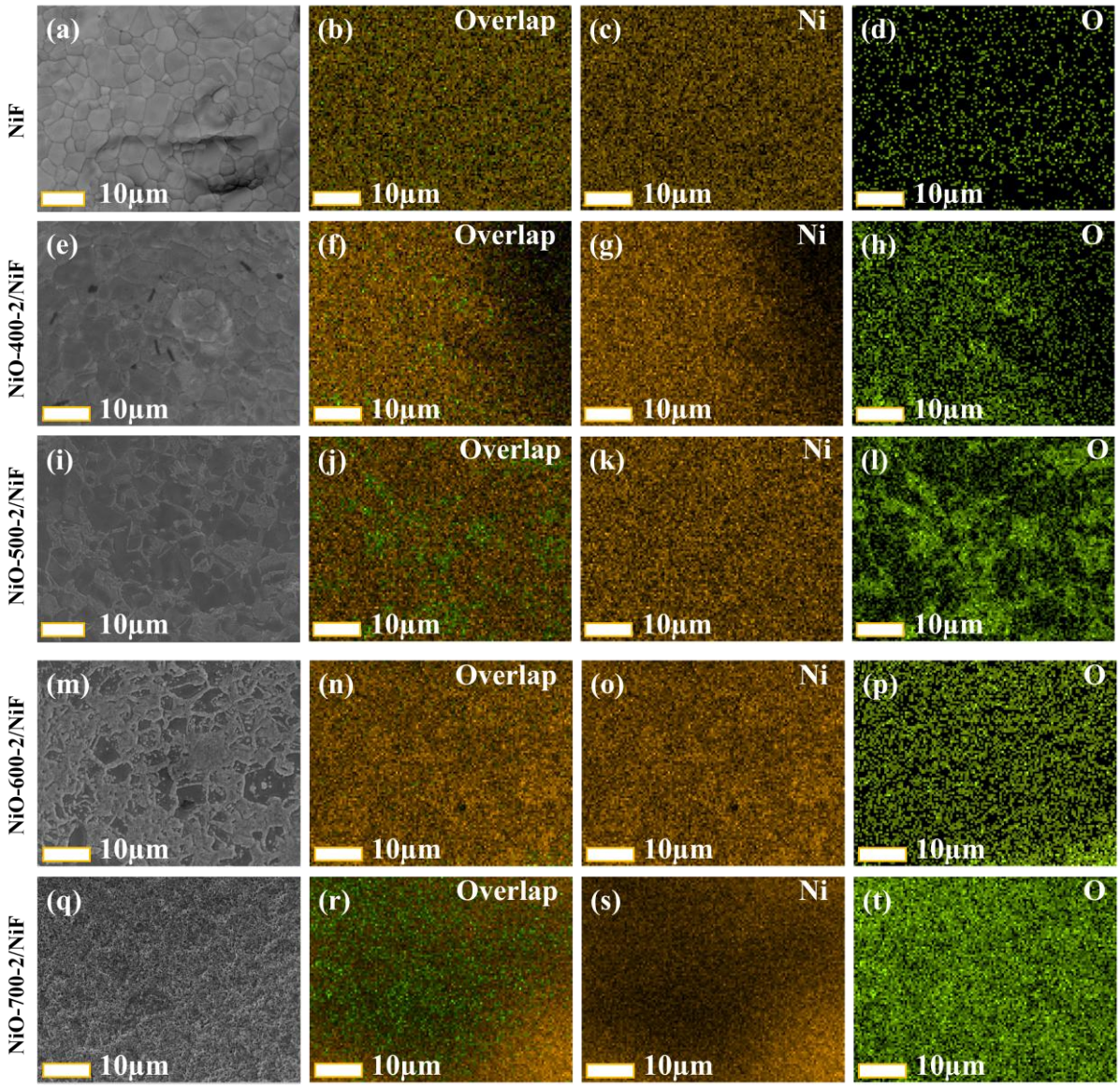

Figure 4. 3 EDS images of NiO/NiF films oxidized at different thermal condition (a-d) Bare Nickel Foam (e-h) NiO-400-2/NiF (i-l) NiO-500-2/NiF (m-n) NiO-600-2/NiF (q-t) NiO-700-2/NiF

The EDS images of NiO-600-2/NiF shows higher amount of oxidation on NiF surface having uniform distribution of Ni and O in Fig.4.3(m-p). The elemental mapping shows increased amount of oxygen that suggests higher amounts of NiO due to oxidation compared to NiO-400-2/NiF and NiO-500-2/NiF. A higher amount of NiO on NiF substrate is advantageous for the performance of the catalytic activity in OER reaction.

The EDS maps of NiO-700-2/NiF Fig.4.3 (q-t) reveal a higher degree of oxidation compared to NiO-500-2/NiF and NiO-600-2/NiF, with a dense and thick NiO layer covering the foam surface. The amount of Ni altered much more by oxygen, indicating a thick and excessive NiO layer. The oxygen content is significantly higher, with a corresponding decrease in porosity and Ni surface contact. While the increased NiO coverage provides abundant active sites for OER, the excessive oxidation negatively impacts HER due to reduced conductivity and impaired electron transfer. The thick oxide layer also limits the accessibility of the active sites, reducing the porosity that results in overall low performance.

4.4 OER performance of thermally modified NiF at different temperature

Oxygen evolution reaction performance of different samples has been evaluated using Linner swept voltammetry (LSV) at a scan rate of 5 $mVdec^{-1}$ in a three-electrode system. The NiO-600-2/NiF sample, which is thermally treated at 600 °C for 2 hours, exhibits the best performance for OER among the five samples followed by NiO-400-2/NiF, NiO-500-2/NiF, NiO-700-2/NiF, and Bare NiF respectively Fig. 4.4(a). Current density is observed increasing significantly with the increase of applied potential, that indicates the OER activity of electrode samples.

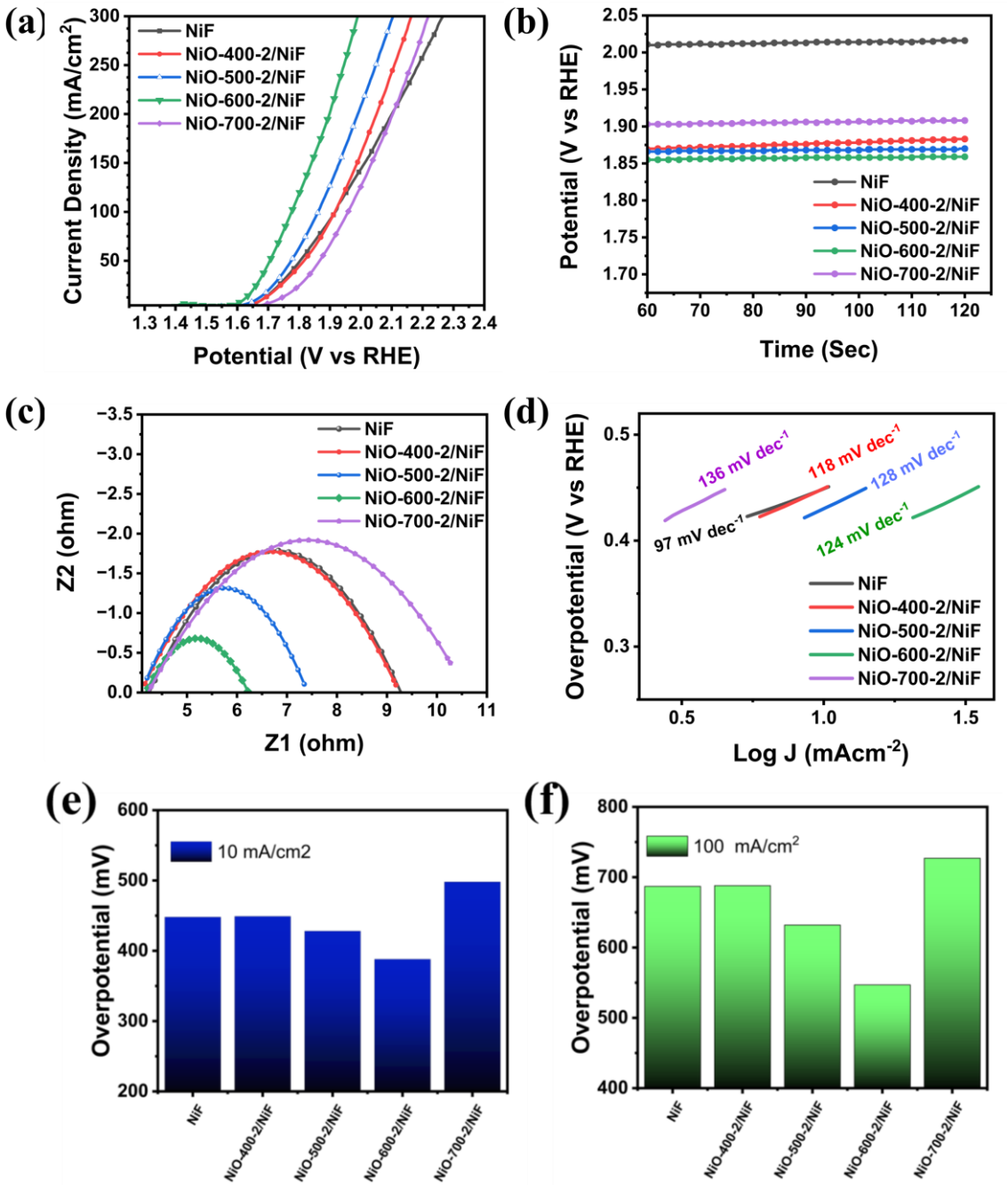

Figure 4. 4 (a) LSV curves of NiO/NiF at a scan rate of 5 mVs-1 (b) Durability curve of NiO/NF at constant current (c) Nyquist plot (d) Tafel slope for OER (e) Overpotential at current density of 10 mAcm-2 (f) Overpotential at current density of 100 mAcm-2.

The NiO-600-2/NiF shows the highest current density across the potential range, pointing to the superior OER activity among the five samples. The NiO-600-2/NiF sample exhibits the lowest overpotential of 388 mV for current density 10mA/cm^2 and 547mV for the current density 100 mA/cm^2. While other samples show higher overpotential at both current density of 10 mA/cm^2 and 100 mA/cm^2 Fig 4.4 (e-f). At the current density of 10 mAcm^{-2}, the overpotential for NiO-600-2/NiF is 388 mV whereas the overpotential for Bare NiF, NiO -400-2/NiF, NiO-500-2/NiF, and NiO -700-2/NiF are 449 mV, 448 mV, 430 mV and 499 mV respectively. At the current density of 100 mAcm^{-2}, the overpotential for NiO -600-2/NF is 547 mV whereas the overpotential for Bare NF, NiO-400-2/NiF, NiO-500/NiF, and NiO-700-2/NF are 687 mV, 688 mV, 632 mV and 727 mV respectively.

The chronopotentiometry results in Fig. 4.4 (b) also show the same trend as LSV result, showing the NiO-600-2/NiF sample requires the lowest potential to maintain current density of 100 mA/cm^2. The sample NiO-400-2/NiF, NiO-500-2/NiF, NiO-700-2/NiF and NiF exhibits a trend of requiring higher potential to maintain same current density of 100 mA/cm^2.

In Fig.4.4 (d) the Tafel plots shows that the NiO-600-2/NiF has a Tafel slope of 124 mV dec^{-1}, which is lower than NiO-400-2/NiF (118 mV dec^{-1}), NiO-500-2/NiF (128 mV dec^{-1}), NiO-700-2/NiF (136 mV dec^{-1}) and NiF (97 mV dec^{-1}). The lower Tafel slope value of NiO-600-2/NiF suggests faster catalytic kinetics of this electrode for OER. Furthermore, electrochemical impedance spectra (EIS) were performed to study the charge transfer kinetics of NiF and modified samples. In Fig4.4 (c), NiO-700-2/NiF shows the higher charge transfer resistance (R_{ct}) 2.35 ohm, while NiO-400-2/NiF, NiO-500-2/NiF, NiO-700-2/NiF and NiF shows 5.02 ohm, 3.14 ohm, 6.17 ohm and 5.14 ohm respectively.

4.5 HER performance of thermally modified NiF at different temperature

HER performance of different samples has been evaluated using Linner swept voltammetry at a scan rate of 5 mVdec^{-1} in a three-electrode system. The NiO-500-2/NiF which is thermally treated at 500 °C for 2 hours, exhibits the best performance for HER among the five samples in Fig. 4.5 (a).

From the polarization curve it is derived that NiO-500-2/NiF requires only 160 mV to deliver 10 mA/cm^2, which is 251 mV, 272 mV, 289 mV and 311 mV for NiO-600-2/NiF, NiO-400-2/NiF, NiF and NiO-700-2/NiF respectively. At the higher current density 100 mA/cm^2, the NiO-500-2/NiF also needs lowest potential among the samples, that is 377 mV, while NiO-600-2/NiF, NiO-400-2/NiF, NiF and NiO-700-2/NiF requires 476 mV, 535 mV, 511 mV and 551 mV respectively. The chronopotentiometry plot reveals the performance of electrode sample by potential (V vs RHE) vs time in Fig. 4.5 (b). IT shows also NiO-500-2/NiF electrode need consistently lowest potential, pointing out stable performance. Stability of NiO-600-2/NiF and NiO-500-2/NiF follows the best sample respectively.

Nyquist plot in Fig.4.5 (c) shows NiO-500-2/NiF has the lowest semicircle, indicating lowest charge transfer resistance (R_{ct}) that is 1.5 ohm. In Fig.4.5 (d) the Tafel plot shows that the NiO-500-2/NiF has a Tafel slope of 106 mV dec^{-1}, which is lowest among the samples, that supports the best performance of the sample for HER. The plot exhibits NiO-600-2/NiF, NiO-400-2/NiF (178 mV dec^{-1}), NiO-700-2/NiF (141 mV dec^{-1}) and NiF have Tafel slope of 125 mV dec^{-1}, 178 mV dec^{-1}, 141 mV dec^{-1} and 128 mV dec^{-1} respectively. The lower Tafel slope value of NiO-500-2/NiF suggests faster catalytic kinetics of this electrode for HER.

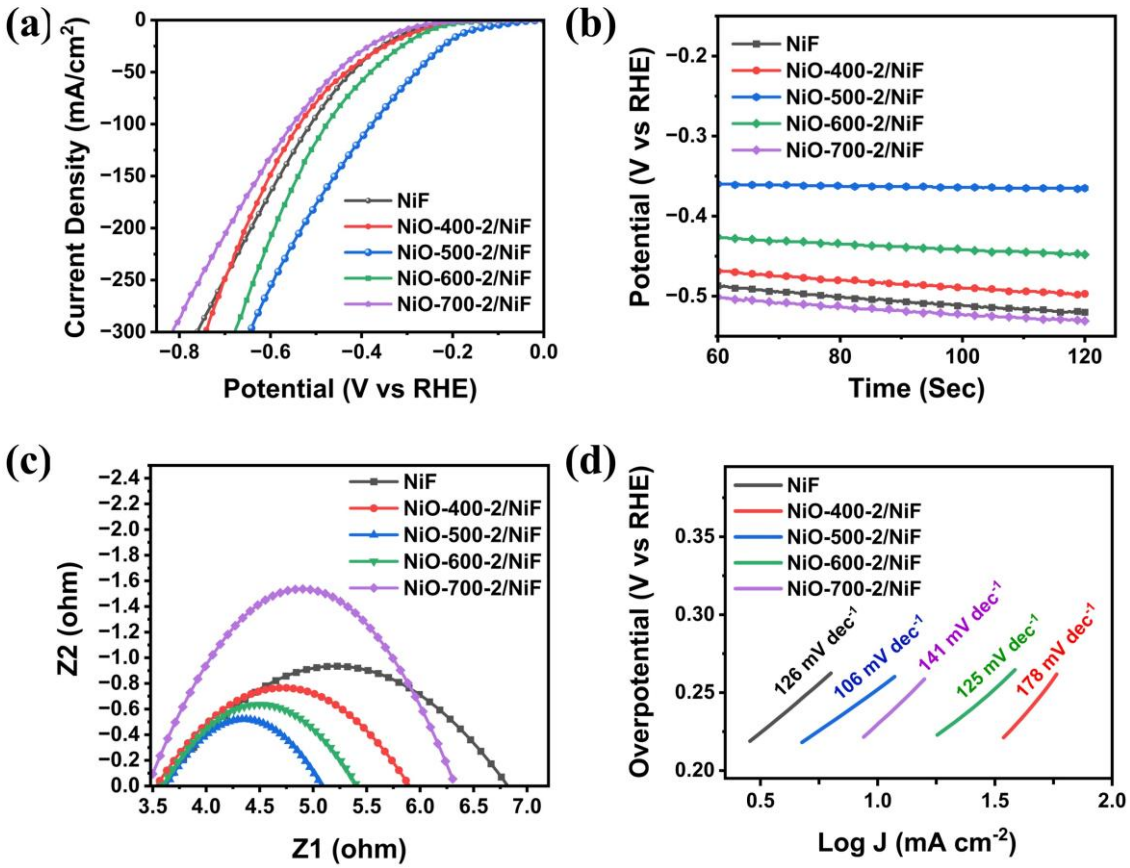

Figure 4. 5 (a) LSV curves of NiO/NiF samples of different temperature at a scan rate of 5 mVs-1 (b) Durability curve of NiO/NiF NiO/NiF samples of different temperature at constant current supply (c) Nyquist plot of NiO/NiF samples of different temperature at 50mA

From the electrochemical test of samples for the duration of two hours, as NiO-500-2/NiF and NiO-600-2/NiF showed best HER and OER performance respectively among the samples, these two samples were selected for further study. In that process, further samples are prepared considering duration ranges 30 mins to 4 hours for both 500 C and 600 C. Later a sample at temperature 500° C for duration of 15 min was considered for extensive study.

Table 2. Description further of thermal treatment of NiF changing duration

Sample Number	**Sample name**	**Thermal treatment temperature** (° C)	**Duration** (Hours)
1	NiO-500-.25/NiF	500	0.25
2	NiO-500-.5/NiF	500	0.5
3	NiO-500-1/NiF	500	1
4	NiO-500-4/NiF	500	4
5	NiO-600-.5/NiF	600	0.5
6	NiO-600-1/NiF	600	1
7	NiO-600-4/NiF	600	4

4.6 XRD Analysis of thermally modified NiF at 600° C at different duration.

The XRD patterns of nickel foam samples (NiO-600-.5/NiF, NiO-600-1/NiF, NiO-600-2/NiF and NiO-600-4/NiF) exhibit peaks corresponding to the cubic phase of nickel oxide (NiO), which appear at 2θ angle = 37.2°, 43.3°, 62.9°, 75.4° and 79.4°, are assigned to the (111), (200), (220), (311), and (222) planes of NiO, respectively, based on the reference data in JCPDS card 89-7131. In the XRD pattern of NiO-600-.5/NiF in Fig. 4.6 (a) , there is visible peaks for NiO at the 37.2°, 43.3°, 62.9° which became stronger in NiO-600-1/NiF, NiO-600-2/NF and NiO-600-4/NF sample respectively. The NiO-600-4/NF shows the stongest peaks for 37.2°, 43.3°, 62.9°, 75.4° and 79.4° in Fig. 4.6 (a) indicating that this sample contains highest amount of NiO among the sample. If XRD pattern of samples are compared from NiO-600-.5/NiF to NiO-600-4/NiF, it is evident that the Ni peak in the sample treated for longer duration (NiO-600-4/NiF) has a short peak of nickel (JCPDS 1-1260) than that of (NiO-600-.5/NiF), that suggests when there is formation of more NiO for comparative long duration thermal treatment, the sample lose Ni from its surface for the NiO formation. In Fig.4.6 (b) & (c) significant shift of Ni peak is observed at 2Θ angles of 44.5° and 76.4° that suggest formation of new composition while intensity peak at at 2Θ angle 43.3° increases that suggest formation of NiO on NiF surface.

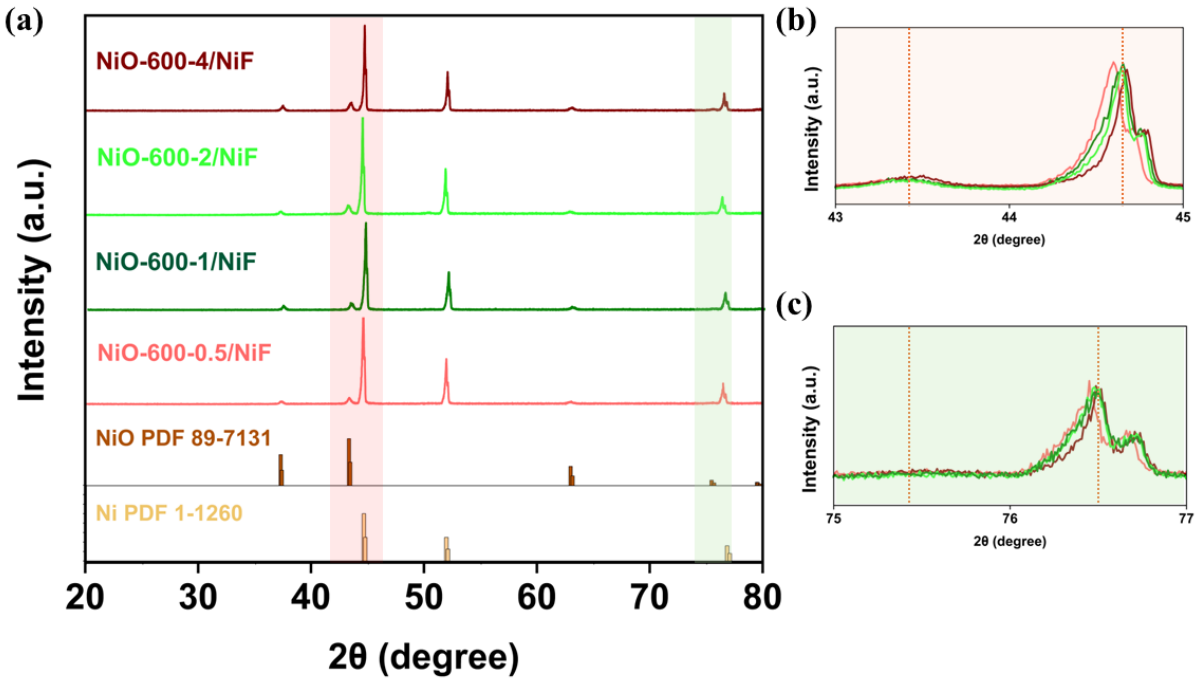

Figure 4. 6 (a). XRD pattern of nickel oxide (NiO) on NF substrate after oxidation at different durations at 600°C temperatures. (b) Overlapping of peaks for (43 ~ 45) 2Θ degree (c) Overlapping of peaks for (75 ~ 77) 2Θ degree.

4.7 Morphology analysis of thermally modified NiF at 600° C at different duration.

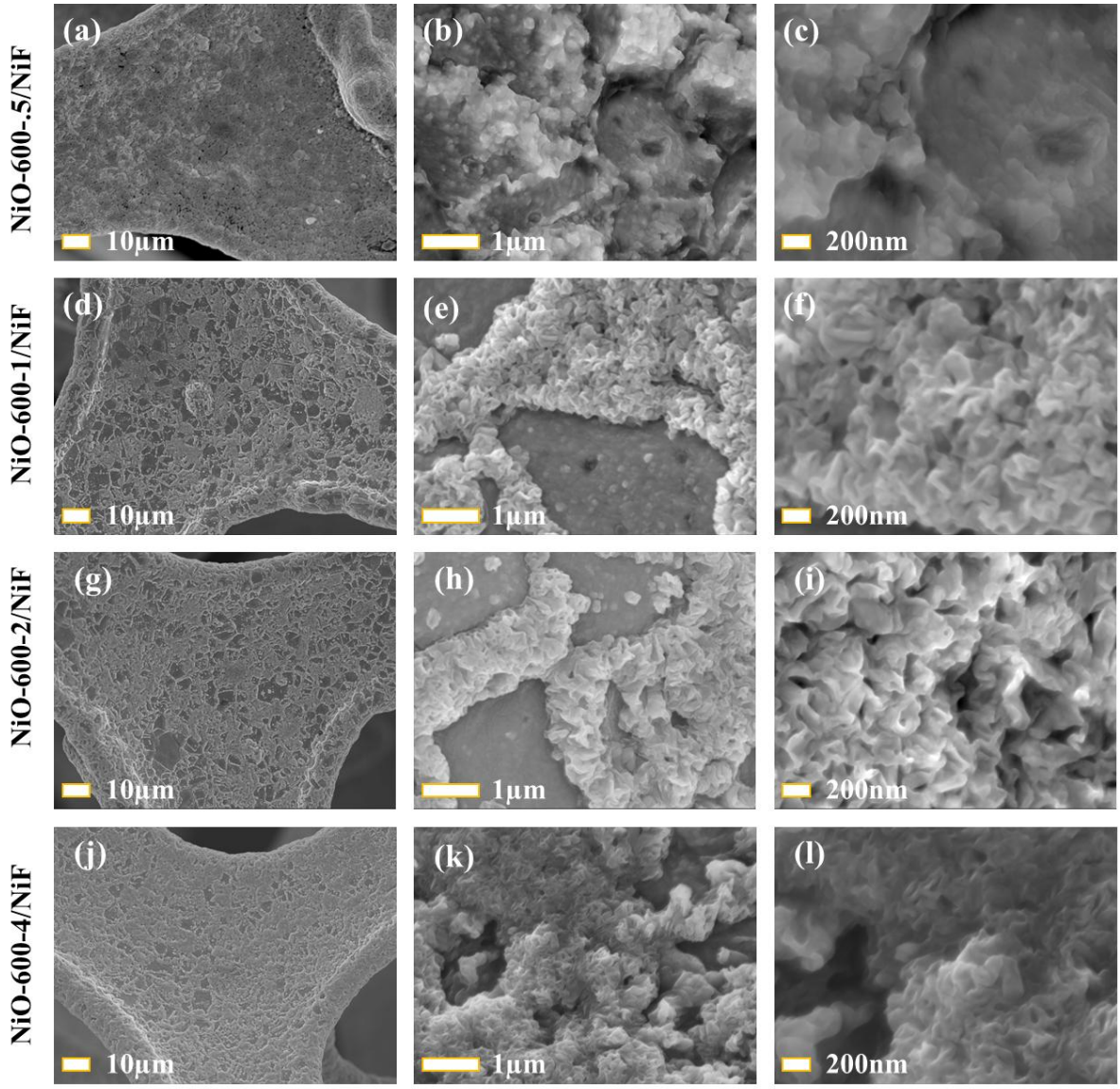

Figure 4. 7 FE-SEM images of NiO/NiF films oxidized at different thermal condition (a-c) NiO-600-.5/NiF (d-f) NiO-600-1/NiF (g-i) NiO-600-2/NiF (j-l) NiO-600-4/NiF

The SEM images of NiO-600-0.5/NiF in Fig. 4.7(a-c) depict a relatively thin and incomplete oxide layer with a smooth surface compared to other samples. While some nanoscale features are visible, the surface appears less porous and less developed. Limited porosity and incomplete oxidation reduce the number of accessible active sites, resulting in lower catalytic activity for OER. The smooth morphology indicates insufficient thermal exposure, which hinders the growth of a well-defined NiO layer critical for improving OER performance.

The sample oxidized for 1 hour (NiO-600-1/NiF) retains a well-defined 3D porous structure, as shown in Fig 4.7(d-f), with minimal distortion to the foam network. Image analysis indicates the sample has a high porosity percentage (~70%), facilitating better electrolyte accessibility to the active sites. The surface is covered with a thin and uniform NiO layer, contributing approximately 40-45% of the total surface area. Although the NiO layer is not as thick as in the samples oxidized for longer durations, the combination of high porosity and optimal NiO coverage enhances the electrochemical active surface

area. This balance between porosity and oxide coverage supports efficient mass transport and rapid charge transfer during OER, making NiO-600-1/NiF the most effective electrocatalyst in experimental results. Babal et al,2018 found similar results in their study[16].

Oxidation for 2 hours (NiO-600-2/NiF) results in a denser oxide layer and slightly reduced porosity (~65%), as observed in Fig 4.7(g). The NiO layer is more developed and covers approximately 45-55% of the surface area. While the increased NiO content provides a greater number of active sites, the reduced porosity hinders electrolyte penetration, which can negatively affect mass transport. At higher magnifications Fig 4.7(h-i), the grains are larger and more interconnected, increasing surface roughness. However, the trade-off between thicker oxide coverage and reduced porosity limits the overall efficiency of the OER, as the accessibility of the electrolyte and ion diffusion is somewhat compromised.

The sample oxidized for 4 (NiO-600-4/NiF) hours exhibits a thicker and more aggregated NiO layer, covering approximately 50-60% of the surface area, as shown in Fig 4.7(j). However, the porosity decreases significantly to ~60% as the denser oxide layer fills the pores of the nickel foam. The excessive NiO aggregation observed in Fig 4.7(k-l) results in larger grains that reduce the effective number of exposed active sites. The dense oxide layer also impairs electron and ion transfer during the OER, further reducing catalytic performance. While the thicker NiO layer may increase activity, it sacrifices the balance between porosity and active site accessibility, leading to reduced OER activity compared to the 1-hour oxidized sample.

4.8 Elemental composition analysis of thermally modified NiF at 600° C at different duration

The EDS elemental maps of NiO-600-.5/NiF reveal significant differences in elemental distribution among the NiO/NiF films oxidized at 600°C varying duration from 0.5 to 4 hour. The NiO-600-.5/NiF reveals porous hole in Fig4.8(a-d). The EDS images of NiO-600-.5/NiF indicates incomplete oxidation for low duration thermal treatment. The sample NiO-600-1/NiF shows comparatively higher growth in NiO layer in Fig4.9 (e) and high amount of oxygen element in Fig4.8(e-h). Increased oxygen suggests further growth in NiO layer, reducing porous hole in NiF surface. Fig4.8(i-l) shows increased amount of oxygen element and further grown NiO layer in NiO-600-2/NiF sample. The NiO-600-4/NiF sample shows the highly dense and rough layer of NiO depicting Ni and O elements in Fig4.8(m-p).

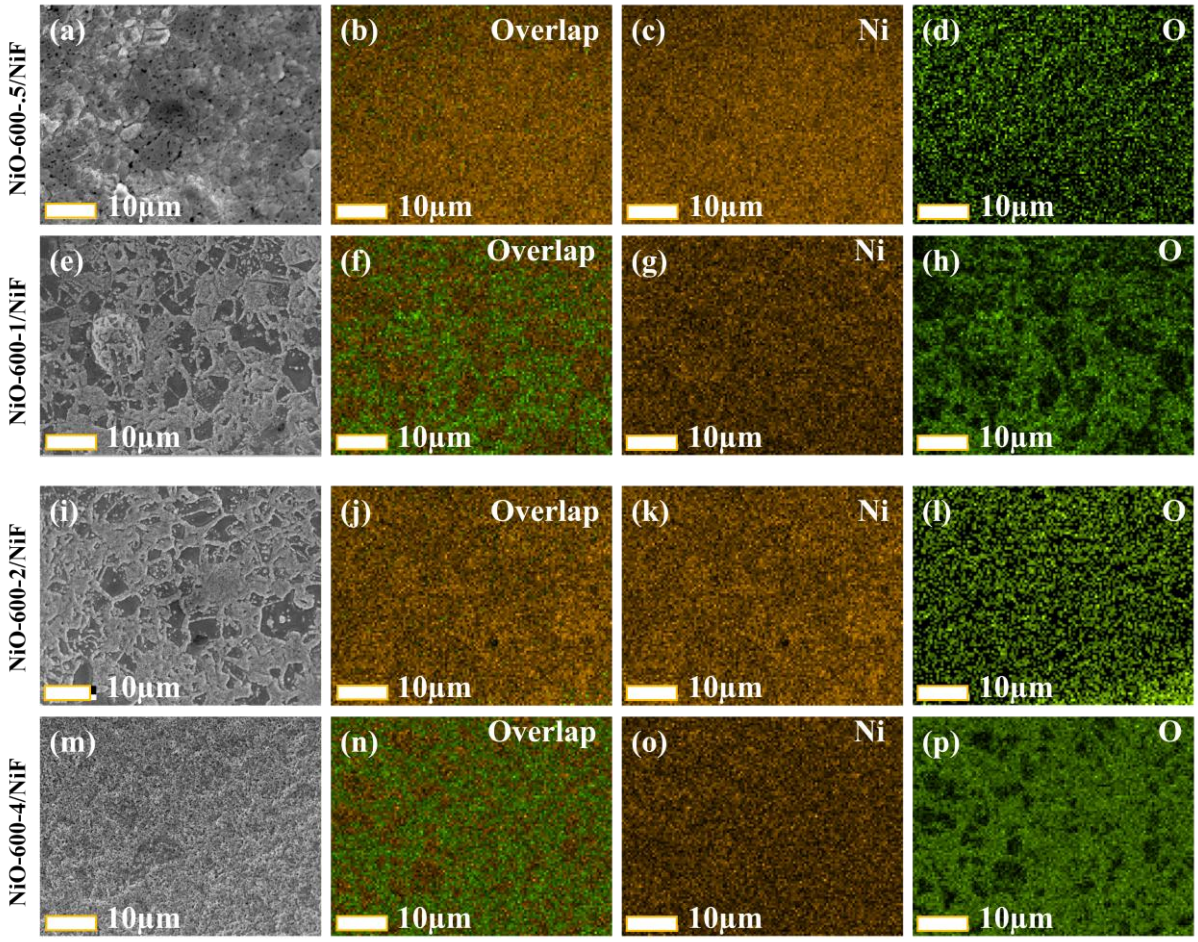

Figure 4. 8 EDS images of NiO/NiF films oxidized at different thermal condition (a-d) NiO-600-.5/NiF (e-h) NiO-600-1/NiF (i-l) NiO-600-2/NiF (m-p) NiO-600-4/NiF

4.9 OER analysis of thermally modified NiF at 600° C at different duration

As a part of further study, the samples thermally treated in 600° C for different duration have been investigated for OER performance, the results are demonstrated in Fig.4.9. The LSV plot in Fig.4.9(a) shows that the NiO-600-1/NiF sample has the best OER performance both at low current density and high current density. At the benchmark of low current density 10mA/cm^2, the NiO-600-1/NiF requires the lowest overpotential of 377mV, while for the same NiO-600-2/NiF, NiO-600-4/NiF and NiO-600-.5/NiF requires higher overpotential of 390mV, 408mv and 407mV respectively. At the higher current density 100mA/cm^2, NiO-600-1/NiF also requires the lowest overpotential of 514mV, where NiO-600-2/NiF, NiO-600-4/NiF and NiO-600-.5/NiF requires the overpotential of 546mV, 583 mV and 593mV respectively. The chronopotentiometry test performed at 100mA in Fig.4.9(b) also shows that the NiO-600-.1/NiF sample requires consistently lowest potential for maintaining same amount of current density indicating best performance among the sample. The Nyquist plot in in Fig.4.9(c), the NiO-600-.1/NiF sample has smallest semicircle which refers to the lowest charge transfer resistance that results in higher OER performance. The NiO-600-4/NiF has the largest semicircle pointing out the highest amount of charge transfer resistance among the sample. The Nyquist plot of NiO-600-.5/NiF has larger semicircle than that of NiO-600-1/NiF, which refers to having higher R_{ct}, that results overall low OER performance. Though the sample NiO-600-2/NiF has an OER performance that follows best

performance among samples, in Nyquist plot it exerts higher R_{ct}, which is indicative for the OER performance degradation at high current density.

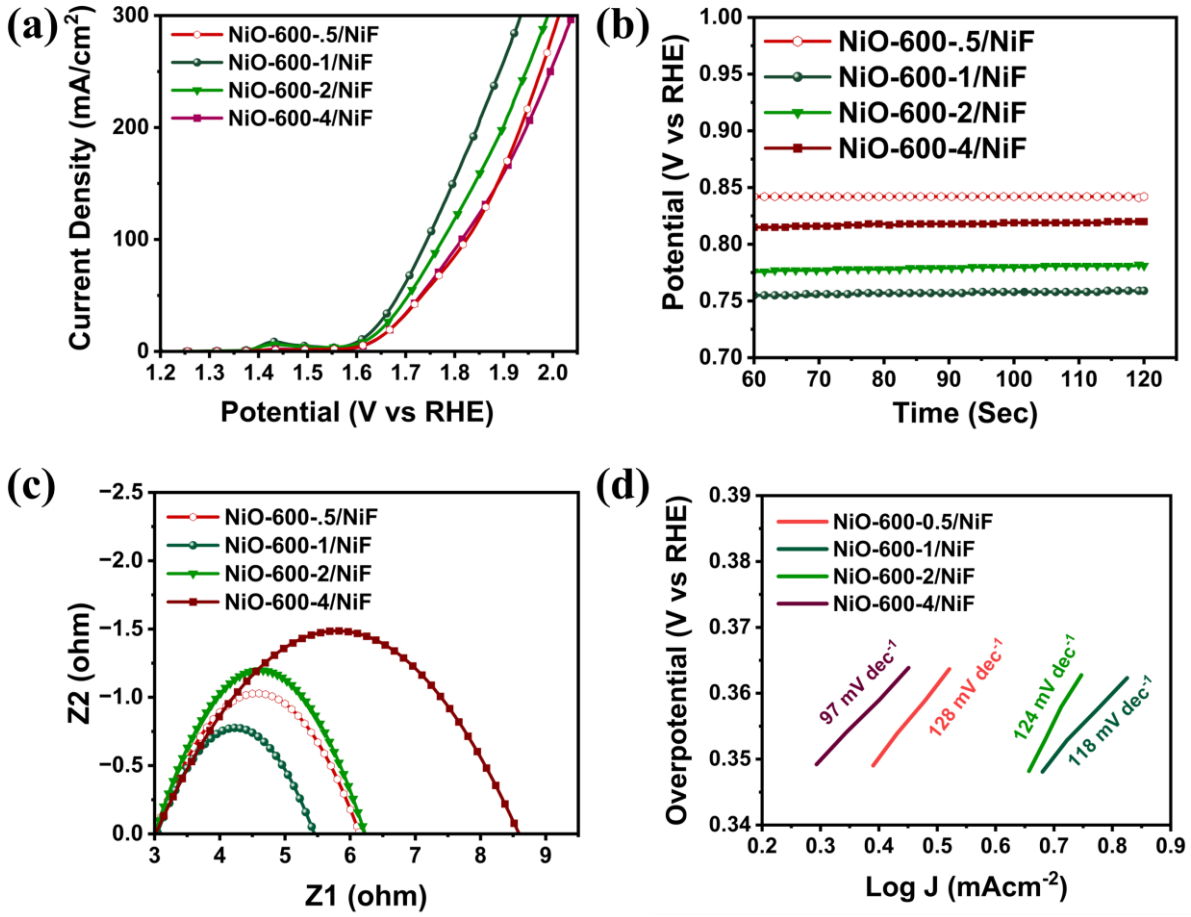

Figure 4. 9 (a) LSV curves of NiO/NiF at 600° C and different duration ranging from 0.5 hour to 4 hour at scan rate of 5 mVs-1 (b) Durability curve of NiO/NF at constant current (c) Nyquist plot (d) Tafel slope for OER

Considering the obtained results from LSV, CP, EIS and Tafel slope, it is evident that the sample treated at 600° C for the duration of 1 hour (NiO-600-1/NiF) has the best performance for oxygen evolution reaction (OER) having overpotential 377mV and 514mV for low and high current density respectively.

4.10 XRD Analysis of thermally modified NiF at 500C at different duration.

The XRD patterns of nickel foam samples (NiO-500-.25/NiF, NiO-500-.5/NiF, NiO-500-1/NiF, NiO-500-2/NiF and NiO-500-4/NiF) exhibit peaks corresponding to the cubic phase of nickel oxide (NiO) in Fig.4.10(a), which appear at 2θ angle = 37.2°, 43.3°, 62.9°, 75.4° and 79.4°, are assigned to the (111), (200), (220), (311), and (222) planes of NiO, respectively, based on the reference data in JCPDS card 89-7131. In the XRD pattern of NiO-500-.25/NiF, there is visible peaks for NiO at the 37.2°, 43.3°, 62.9°

which became stronger in NiO-500-.5/NiF, NiO-500-1/NiF, NiO-500-2/NF and NiO-500-4/NF sample respectively. The NiO-500-4/NF shows the stongest peaks among the sample at 2Θ angle of 37.2°, 43.3°, 62.9° in Fig. 4.10(a) indicating that this sample contains highest amount of NiO. If XRD pattern of samples compare from NiO-500-.25/NF to NiO-500-4/NF, it is evident that the Ni peak in the sample treated for longer duration (NiO-500-4/NF) has a decreased intensity of Ni at 2Θ angle 44.5° (JCPDS 1-1260) than that of (NiO-500-.25/NF), that suggests when there is formation of more NiO for comparative long duration thermal treatment, the sample lose Ni from its surface for the NiO formation. In Fig.4.10 (b) & (c) Significant peak intensity shift is observed at 2Θ angle 44.5° and 76.4° respectively, suggesting formation of NiO.

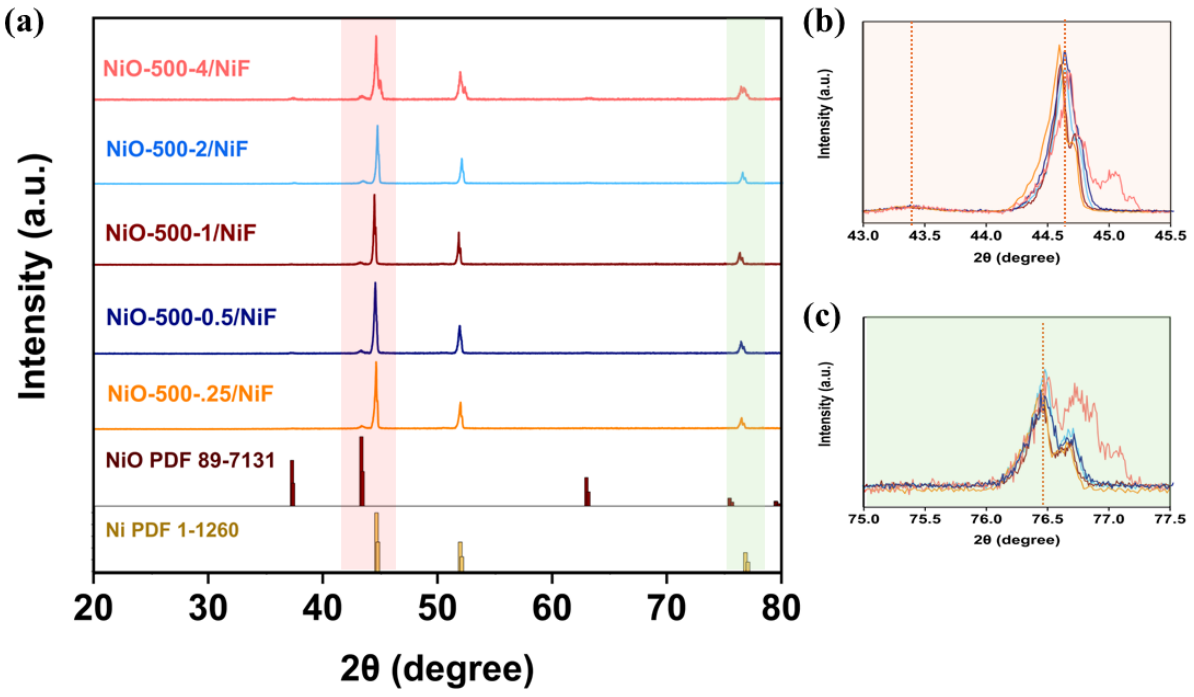

Figure 4. 10 (a). XRD pattern of nickel oxide (NiO) on NF substrate after oxidation at different duration at 500°C temperatures. (b) Overlapping of peaks for (43 ~ 45.5) 2Θ degree (c) Overlapping of peaks for (75 ~ 77.5) 2Θ degree.

4.11 Morphology analysis of thermally modified NiF at 500C at different duration

The SEM images NiO-500-0.25/NiF in Fig 4.11(a-c) reveal a highly porous structure with a porosity of approximately 15–20% and a very thin layer of NiO. This porosity increases the available surface area for catalytic activity, increasing active sites essential for the OER. The combination of optimal porosity and conductive NiO layer provides an ideal platform for efficient electron transfer in oxygen evolution reaction.

The SEM images NiO-500-0.5/NiF in Fig 4.11(d-f) reveal a highly porous structure with a porosity of approximately 35–40% and a moderate layer of NiO. This significant porosity increases the available surface area for catalytic activity, combination of optimum active sites essential for the OER. The combination of optimal porosity and conductive NiO layer provides an ideal platform for efficient electron transfer in oxygen evolution reaction.

The sample oxidized for 1 hour (NiO-500-1/NiF) shows an initial development of the oxide layer. At low magnification Fig 4.11(g), the nickel foam retains its macro-porous 3D network with

minimal surface modifications. However, at higher magnifications Fig 4.11(h-i), the formation of comparatively thick and dispersed NiO grains is observed on the foam's surface. Grains are relatively fine and not densely packed, indicating the early stages of NiO growth. Due to the limited surface roughness observed in morphology, it is expected moderate catalytic activity provided by active sites for electrochemical reactions.

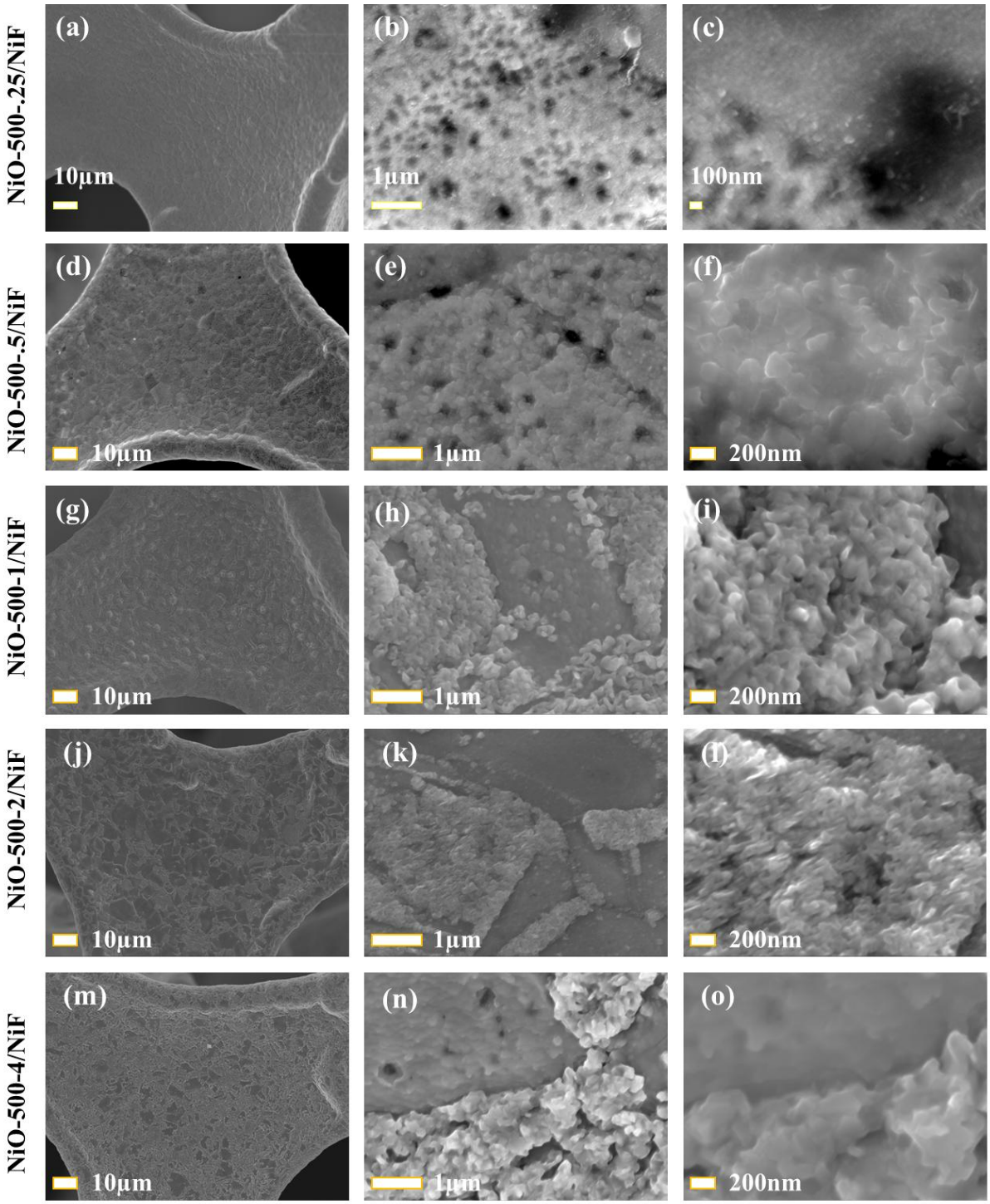

Figure 4. 11 FE-SEM images of NiO/NiF films oxidized at different thermal condition (a-c) NiO-500-.25/NiF (d-f) NiO-500-.5/NiF (g-i) NiO-500-1/NiF (j-l) NiO-500-2/NiF (m-p) NiO-500-4/NiF

The 2-hour oxidation at 500 C sample (NiO-500-2/NiF) shows a significant change in morphology. The porous network of the nickel foam is preserved Fig 4.11(j), but the surface is now covered with a denser and more uniformly distributed NiO layer, as seen in images Fig 4.11(k-l). The NiO grains have grown larger, forming a textured surface with an increased surface area. Though this nanostructured oxide layer should have increased the material's catalytic activity due to the increased oxide layer, it has reduced active sites by covering the porous nano-holes on the surface, affecting its activity for the hydrogen evolution reaction (HER).
After 4 hours of oxidation at 500 C of sample (NiO-500-4/NiF), the NiO layer becomes thicker and more compact, as shown in images Fig 4.11(m-n). The higher magnification images reveal larger and more aggregated oxide grains Fig 4.11(o). While the prolonged oxidation increases the oxide layer thickness, it produces excessive grain agglomeration, reducing the accessibility of active sites. Additionally, the thicker and denser oxide layer hinders electrical conductivity by reducing porosity, potentially lowering the electrocatalytic efficiency for OER & HER in water-splitting applications.

4.12 Elemental composition analysis of thermally modified NiF at 500C at different duration

The EDS maps of NiO-500-.25/NiF Fig.4.12(a-d) demonstrate the formation of a very thin layer of nickel oxide (NiO) and smoother surface due to removal of surface contaminants by thermal exposure. Porous holes resulted from thermal treatment are visible and that is advantageous for HER. Oxygen is detected in greater amounts compared to the bare foam, but the proportion of NiO remains relatively low compared to other samples. The images depicts to a slight decrease of Ni amount due to partial oxidation. This reflects the formation of a thin NiO layer while retaining a significant metallic Ni core. The incomplete oxidation limits the availability of catalytically active sites, potentially leading to low overall performance for HER and OER.
The sample NiO-500-.5/NiF shows an increased number of porous holes in NiF substrate surface in Fig.4.12(e) and high amount of Oxygen presence in elemental mapping images in Fig.4.12(f-h). The indicates higher amounts of NiO formation compared to NiO-500-.5/NiF sample.
Fig4.12(i) shows that porous holes are covered and Fig4.12(j-l) depicts an increase in the amount of oxygen element resulted in thermal treatment of NiO-500-1/NiF. Though NiO layer increased, it covered the porous holes that are crucial in HER performance. Fig4.12(m-p) shows further growth of NiO layer in NiO-500-2/NiF.
NiO-500-4/NiF shows a denser NiO layer in Fig4.12(q) and elemental mapping Fig4.12(r-t) shows the highly dense oxygen element that refers to the result of high temperature thermal modification among the sample.

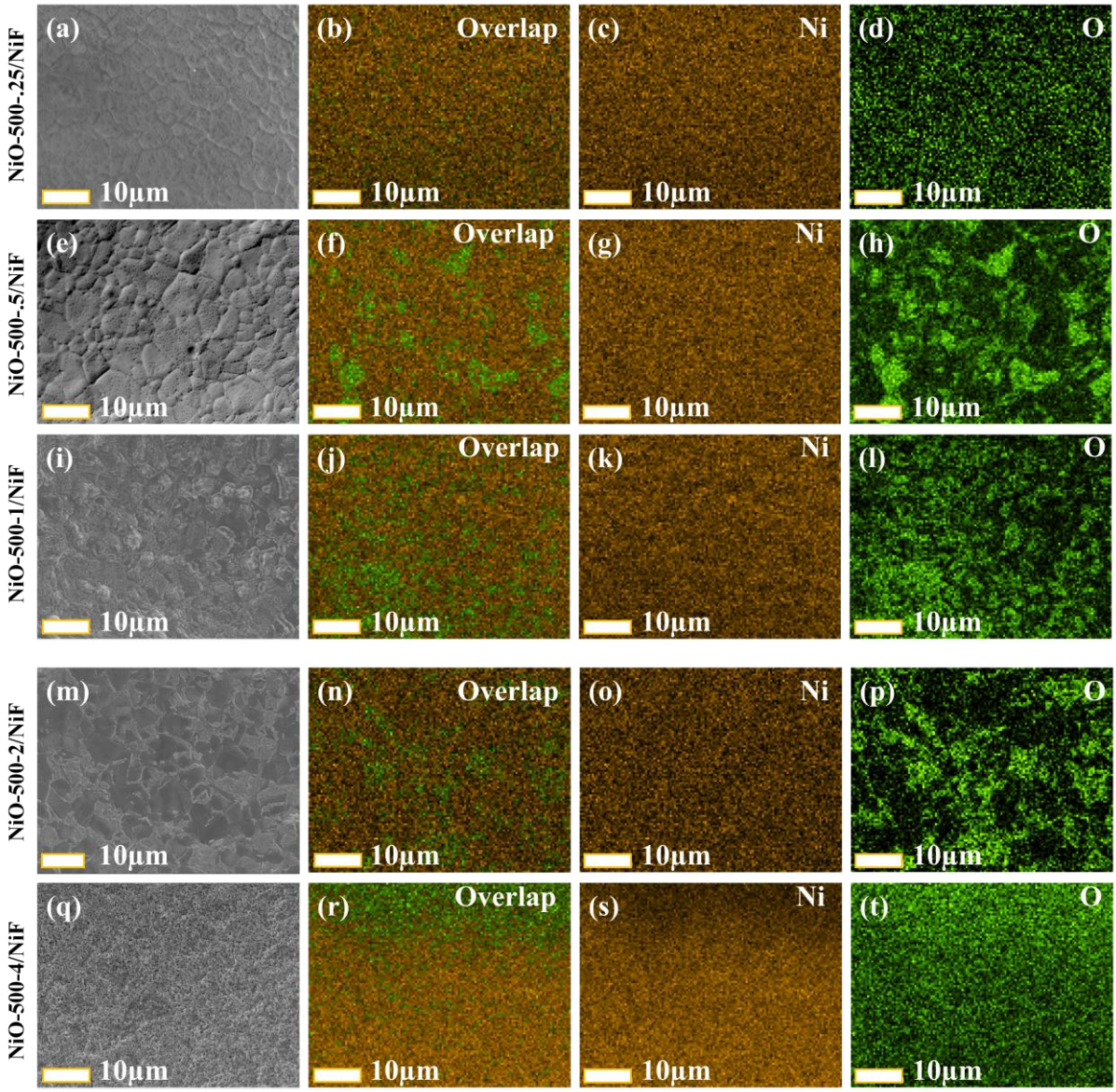

Figure 4. 12 EDS images of NiO/NiF oxidized at different thermal condition (a-d) NiO-500-.25/NiF (e-h) NiO-500-.5/NiF (i-l) NiO-500-1/NiF (m-n) NiO-500-2/NiF (q-t) NiO-500-4/NiF

4.13 HER analysis of thermally modified NiF at 500° C at different duration

In this stage, HER performance of five samples is investigated, where NiO-500-.5/NiF Exhibits the best performance for linear swept voltammetry at a scan rate of 5mV/sec. In Fig. 4.13(a) the NiF-500-.5/NiF depicts that it requires lowest potential both in low and high current density. For the benchmark 10mA/cm^2 NiO-500-.5/NiF sample requires only 146 mV where NiO-500-1/NiF, NiO-500-2/NiF, NiO-500-4/NiF and NiO-500-.25/NiF requires 207mV, 208 mV, 224mV and 258mV respectively. The low performance of NiO-500-.25/NiF is due to insufficient amount of active NiO layer which is result of thermal treatment for very short duration. The chronopotentiometry results in Fig. 4.13(b) also support the result obtained from LSV, that shows NiO-500-.5/NiF sample is consistently requiring the consistent amount of potential for current density of 100mA/cm^2. NiO-500-1/NiF, NiO-500-2/NiF, NiO-500-4/NiF and NiO-500-.25/NiF samples also follow the same trend of performance as LSV in chronopotentiometry. The Nyquist plot obtained from Electrical Impedance Spectroscopy in Fig. 4.13(c) NiO-500-.1/NiF sample has lowest current transfer resistance, where best performing sample NiO-500-.5/NiF has a higher current transfer resistance than that of sample of 1 hour. The NiO-500-.25/NiF sample has shown a larger semicircle than NiO-500-.5/NiF, that indicates comparatively low performance, which is followed by NiO-500-1/NiF and NiO-500-4/NiF.

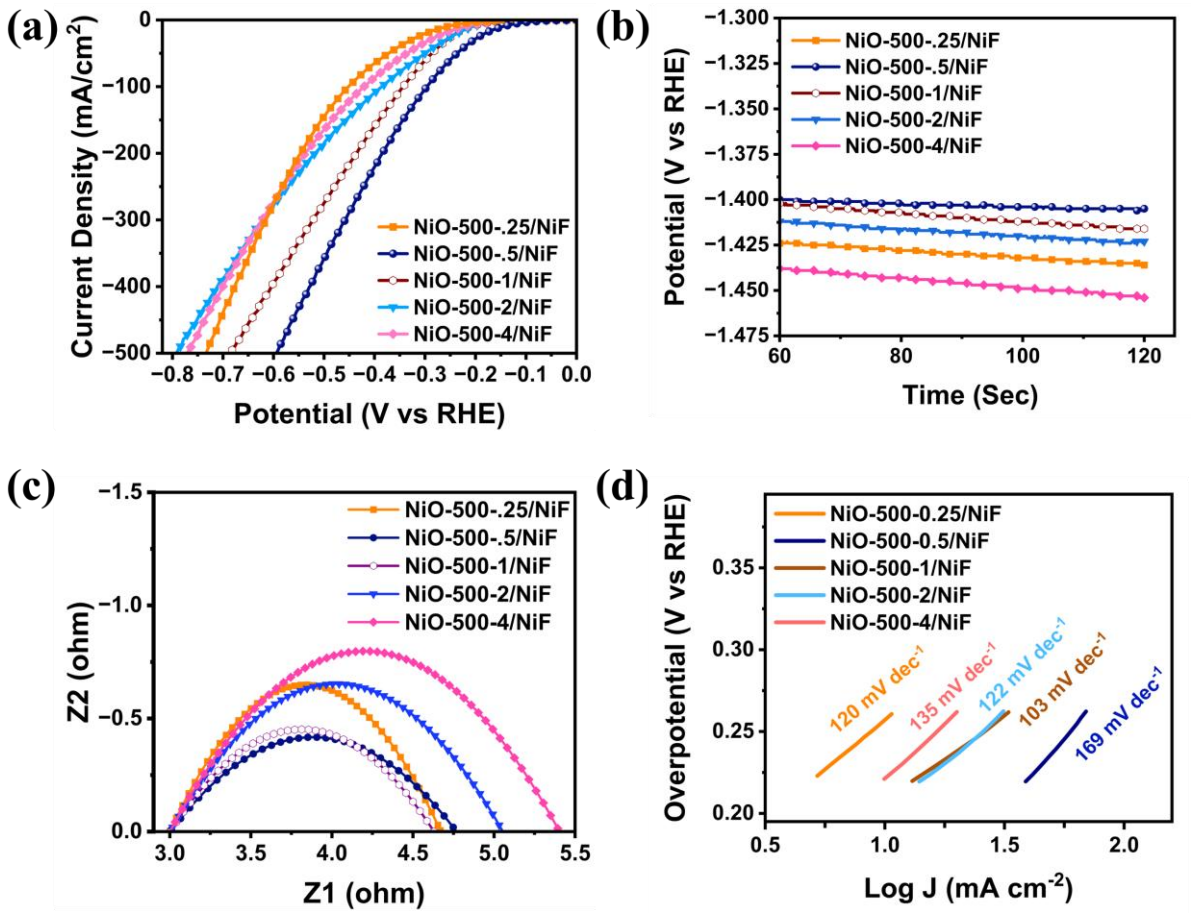

Figure 4.13 (a) LSV curves of NiO-500/NiF samples at different duration at a scan rate of 5 mVs-1 (b) Durability curve of NiO-500/NiF samples at different duration at constant current supply (c) Nyquist plot (d) Tafel slope of NiO-500/NiF samples at different durat

4.14 Comparison of OER and HER performance with benchmark electrodes

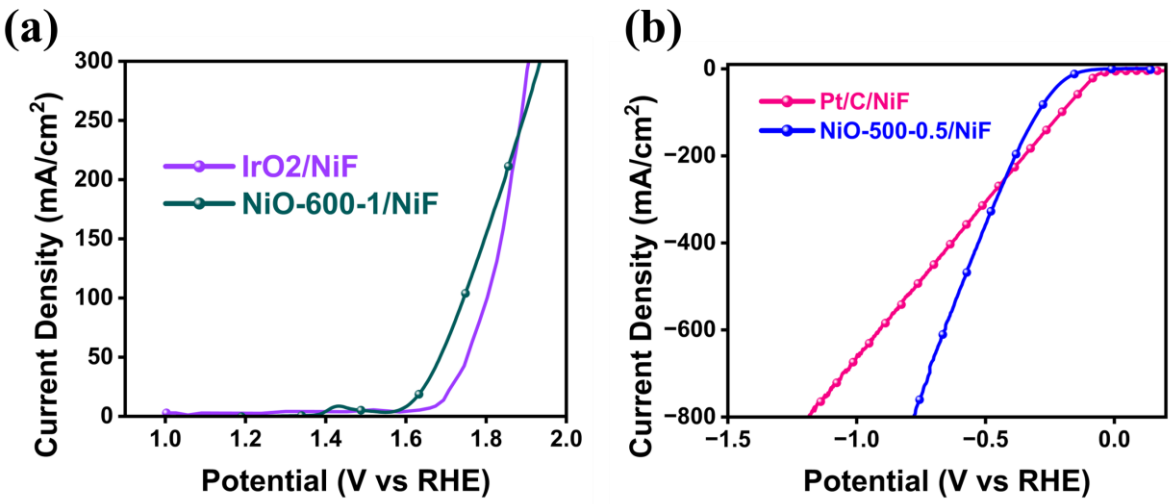

Figure 4. 14 (a) OER LSV of IrO2/NiF and NiF-600-1/NiF (b) HER LSV of Pt/C/NiF and NIO-500-0.5/NiF

The performance of NiO-500-.5/NiF electrode is compared with the performance of Pt/c/NiF for HER and performance of NiO-600-1/NiF is compared with performance of IrO_2/NiF electrode for OER. Fig 4.14 (a) shows that thermally treated NiO-600-1/NiF sample perform better for OER than IrO_2/NiF. NiO-500-0.5/NiF sample also performs better for HER at high current density than Pt/C/NiF.

4.15 Full cell water splitting performance with 1.0 M KOH

Finally, considering the superior HER activity of NiO-500-0.5/NiF and OER activity of NiO-600-1/NiF, two electrode is paired to cathode and anode respectively in a two-electrode cell with 1M KOH as electrolyte solution to monitor overall water splitting. From the result in Fig 4.15(a), we can see that NiO-500-0.5/NiF // NiO-600-1/NiF water electrolyser requires only 1.768 V and 2.221 V to deliver 10mA/cm^2 and 100 mA/cm^2 respectively.

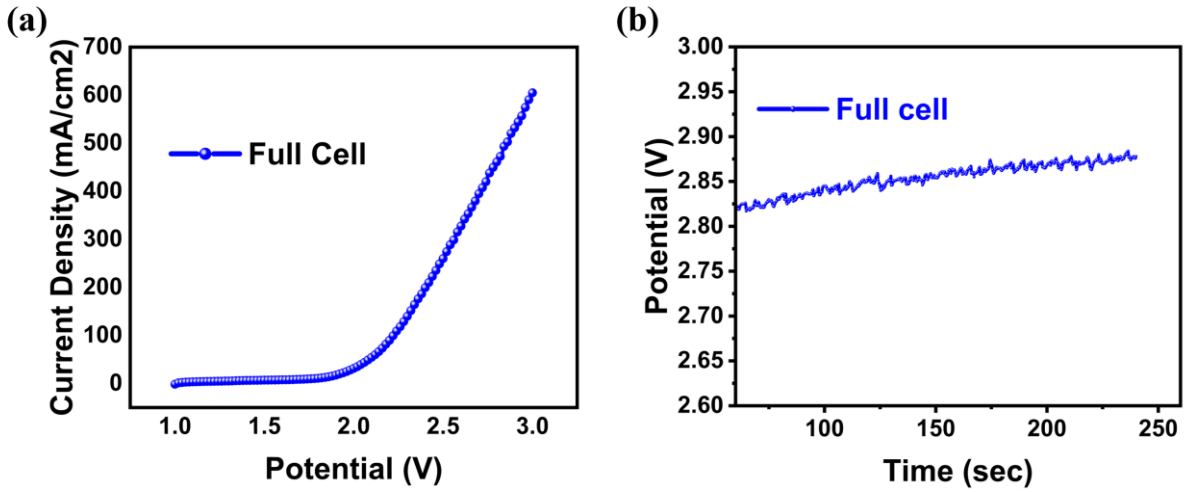

Figure 4. 15 (a) LSV curves of full cell having NiO-500-0.5/NiF at cathode and NiO-600-1/NiF at anode at scan rate of 5 mVs-1 (b) Durability curve of full cell at constant current 100mA.

4.16 Full cell water splitting performance with 6.0 M KOH

The electrocatalytic HER and OER performance of NiO-500-0.5/NiF and NiO-600-1/NiF is further demonstrated in long duration durability test at high current density (500mA/cm^2) . A chronopotentiometry measurement was performed at 500 mA for 250 hours in 6M KOH electrolyte solution using NiO-500-.5/NiF as cathode and NiF-600-1/NiF as anode. Obtained voltages in full cell study are displayed as a function of time in Fig4.16, that depicts it operated in 2.5V with negligible fluctuation/stability. It proves excellent stability and efficient performance of NiF-500-0.5/NiF for HER and NiF-600-1/NiF for OER.

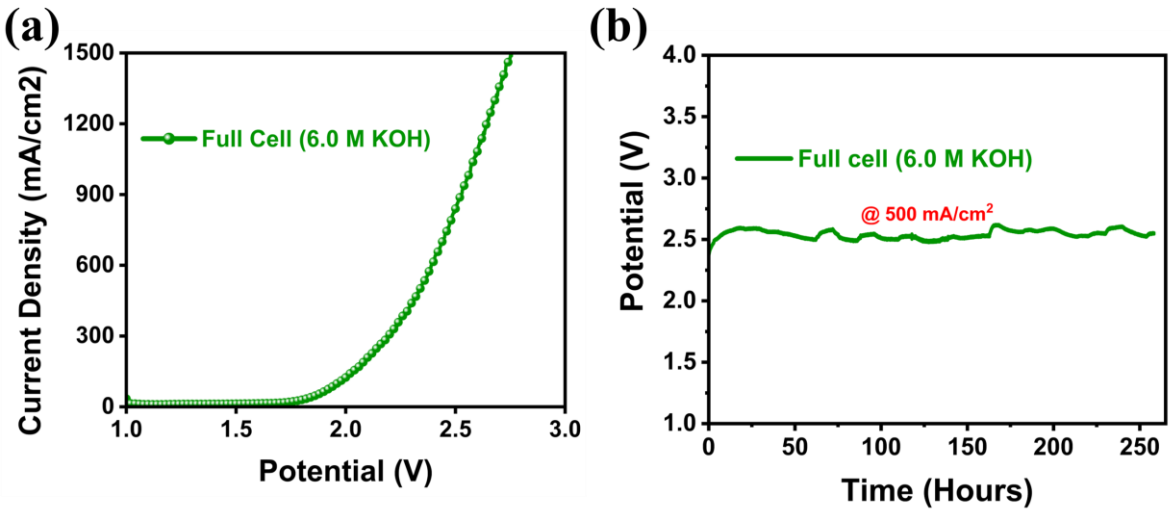

Figure 4. 16 (a) Full cell LSV (b) Durability curve of full cell at constant current 500 mA/cm2.

Conclusion

In summary, we developed a HER and an OER electrode using a simple thermal treatment to produce NiO in NiF substrate. The NiO-600-/1NiF sample which is treated at 600° C for 1 hour exhibits the best electrocatalytic performance for OER reaction with an overpotential 377 mV and 514 mV for the current density of 10 mA/cm^2 and 100 mA/cm^2 respectively along with consistent durability. The NiO-500-0.5/NiF sample which is treated at 500° C for 30 minutes shows the best electrocatalytic performance for HER reaction with an overpotential 146 mV and 296 at the current density of 10mA/cm^2 and 100mA/cm^2 along with excellent durability. In the full cell test, NiO-500-0.5/NiF // NiO-600-1/NiF water electrolyzer requires only 1.768 V and 2.221 V to deliver 10mA/cm^2 and 100 mA/cm^2 respectively. That presents overpotential 538 mV and 991 mV for the current density of 10mA/cm^2 and 100 mA/cm^2 respectively. To investigate the performance in industrial water splitting condition, two developed best performing electrode is observed in a full cell setup with 6.0 M KOH electrolyte solution, where it requires only 2.5 V to achieve 500 mA/cm^2 and exhibits long term durability. This study introduces a cost-effective approach to synthesis bifunctional electrode for overall water splitting which is potential to drive forward the water splitting technology

Recommendations

List of References

[1] A. Vilanova, P. Dias, T. Lopes, and A. Mendes, 'The route for commercial photoelectrochemical water splitting: a review of large-area devices and key upscaling challenges', Jan. 30, 2024, *Royal Society of Chemistry*. doi: 10.1039/d1cs01069g.

[2] N. K. Chaudhari, H. Jin, B. Kim, and K. Lee, 'Nanostructured materials on 3D nickel foam as electrocatalysts for water splitting', Sep. 14, 2017, *Royal Society of Chemistry*. doi: 10.1039/c7nr04187j.

[3] S. Srinivasan, S. Sherif, F. Barbir, T. Veziroglu, M. Mahishi, and R. Pratt, 'Hydrogen Energy Technologies', pp. 1693–1726, Sep. 2015, doi: 10.1201/B18947-58.

[4] S. van Renssen, 'The hydrogen solution?', Sep. 01, 2020, *Nature Research*. doi: 10.1038/s41558-020-0891-0.

[5] Z. P. Ifkovits, J. M. Evans, M. C. Meier, K. M. Papadantonakis, and N. S. Lewis, 'Decoupled electrochemical water-splitting systems: A review and perspective', 2021. doi: 10.1039/d1ee01226f.

[6] L. Ai, Z. Niu, and J. Jiang, 'Mechanistic insight into oxygen evolution electrocatalysis of surface phosphate modified cobalt phosphide nanorod bundles and their superior performance for overall water splitting', *Electrochim Acta*, vol. 242, pp. 355–363, Jul. 2017, doi: 10.1016/J.ELECTACTA.2017.05.032.

[7] N. T. Suen, S. F. Hung, Q. Quan, N. Zhang, Y. J. Xu, and H. M. Chen, 'Electrocatalysis for the oxygen evolution reaction: Recent development and future perspectives', Jan. 21, 2017, *Royal Society of Chemistry*. doi: 10.1039/c6cs00328a.

[8] W. Zhang, D. Li, L. Zhang, X. She, and D. Yang, 'NiFe-based nanostructures on nickel foam as highly efficiently electrocatalysts for oxygen and hydrogen evolution reactions', *Journal of Energy Chemistry*, vol. 39, pp. 39–53, Dec. 2019, doi: 10.1016/J.JECHEM.2019.01.017.

[9] F. Yu, L. Yu, I. K. Mishra, Y. Yu, Z. F. Ren, and H. Q. Zhou, 'Recent developments in earth-abundant and non-noble electrocatalysts for water electrolysis', *Materials Today Physics*, vol. 7, pp. 121–138, Dec. 2018, doi: 10.1016/J.MTPHYS.2018.11.007.

[10] M. D. Bhatt and J. Y. Lee, 'Advancement of Platinum (Pt)-Free (Non-Pt Precious Metals) and/or Metal-Free (Non-Precious-Metals) Electrocatalysts in Energy Applications: A Review and Perspectives', *Energy and Fuels*, vol. 34, no. 6, pp. 6634–6695, Jun. 2020, doi: 10.1021/acs.energyfuels.0c00953.

[11] L. Tan *et al.*, 'Controllable synthesis and phase-dependent catalytic performance of dual-phase nickel selenides on Ni foam for overall water splitting', *Appl Catal B*, vol. 303, p. 120915, Apr. 2022, doi: 10.1016/J.APCATB.2021.120915.

[12] Y. Jiao, Y. Zheng, M. Jaroniec, and S. Z. Qiao, 'Design of electrocatalysts for oxygen- and hydrogen-involving energy conversion reactions', Apr. 21, 2015, *Royal Society of Chemistry*. doi: 10.1039/c4cs00470a.

[13] S. Anantharaj, S. R. Ede, K. Sakthikumar, K. Karthick, S. Mishra, and S. Kundu, 'Recent Trends and Perspectives in Electrochemical Water Splitting with an Emphasis on Sulfide, Selenide, and Phosphide Catalysts of Fe, Co, and Ni: A Review', Dec. 02, 2016, *American Chemical Society*. doi: 10.1021/acscatal.6b02479.

[14] W. T. Hong, M. Risch, K. A. Stoerzinger, A. Grimaud, J. Suntivich, and Y. Shao-Horn, 'Toward the rational design of non-precious transition metal oxides for oxygen

electrocatalysis', May 01, 2015, *Royal Society of Chemistry*. doi: 10.1039/c4ee03869j.

[15] X. Wu, J. Li, Y. Li, and Z. Wen, 'NiFeP-MoO2 hybrid nanorods on nickel foam as high-activity and high-stability electrode for overall water splitting', *Chemical Engineering Journal*, vol. 409, 2021, doi: 10.1016/j.cej.2020.128161.

[16] P. T. Babar, A. C. Lokhande, M. G. Gang, B. S. Pawar, S. M. Pawar, and J. H. Kim, 'Thermally oxidized porous NiO as an efficient oxygen evolution reaction (OER) electrocatalyst for electrochemical water splitting application', *Journal of Industrial and Engineering Chemistry*, vol. 60, 2018, doi: 10.1016/j.jiec.2017.11.037.

[17] M. Yue, H. Lambert, E. Pahon, R. Roche, S. Jemei, and D. Hissel, 'Hydrogen energy systems: A critical review of technologies, applications, trends and challenges', *Renewable and Sustainable Energy Reviews*, vol. 146, p. 111180, Aug. 2021, doi: 10.1016/J.RSER.2021.111180.

[18] A. Gupta, B. Likozar, R. Jana, W. C. Chanu, and M. K. Singh, 'A review of hydrogen production processes by photocatalytic water splitting – From atomistic catalysis design to optimal reactor engineering', *Int J Hydrogen Energy*, vol. 47, no. 78, pp. 33282–33307, Sep. 2022, doi: 10.1016/J.IJHYDENE.2022.07.210.

[19] M. Carmo, D. L. Fritz, J. Mergel, and D. Stolten, 'A comprehensive review on PEM water electrolysis', *Int J Hydrogen Energy*, vol. 38, no. 12, pp. 4901–4934, Apr. 2013, doi: 10.1016/J.IJHYDENE.2013.01.151.

[20] T. B. Ferriday, P. H. Middleton, and M. L. Kolhe, 'Review of the Hydrogen Evolution Reaction—A Basic Approach', *Energies 2021, Vol. 14, Page 8535*, vol. 14, no. 24, p. 8535, Dec. 2021, doi: 10.3390/EN14248535.

[21] M. K. Adak, † Hirak, K. Basak, S. Kumar, and B. Chakraborty, 'Detection of Nickel-oxide Nano-layer During Mild Acid Treatment of Nickel Foam and its Effect on Alkaline Oxygen Evolution and Ammonia Oxidation Reactions'.

[22] N. A. A. Bakar *et al.*, 'The effect different of hydrochloric acid concentrations on the cleaning of Ni foam substrate: Structural and morphological studies', *Mater Today Proc*, vol. 60, pp. 1036–1041, Jan. 2022, doi: 10.1016/J.MATPR.2022.01.227.

[23] T. B. Ferriday, S. Nuggehalli Sampathkumar, P. H. Middleton, J. Van Herle, and M. L. Kolhe, 'How Acid Washing Nickel Foam Substrates Improves the Efficiency of the Alkaline Hydrogen Evolution Reaction', *Energies (Basel)*, vol. 16, no. 5, Mar. 2023, doi: 10.3390/en16052083.

[24] X. Yang *et al.*, 'IrPd Nanoalloy-Structured Bifunctional Electrocatalyst for Efficient and pH-Universal Water Splitting', *Small*, vol. 19, no. 27, 2023, doi: 10.1002/smll.202208261.

[25] S. D. Dhas *et al.*, 'Hierarchical spinel NiMn2O4 nanostructures anchored on 3-D nickel foam as stable and high-performance supercapacitor electrode material', *J Energy Storage*, vol. 71, p. 108168, Nov. 2023, doi: 10.1016/J.EST.2023.108168.

[26] C. Wei *et al.*, 'Recommended Practices and Benchmark Activity for Hydrogen and Oxygen Electrocatalysis in Water Splitting and Fuel Cells', Aug. 01, 2019, *Wiley-VCH Verlag*. doi: 10.1002/adma.201806296.

[27] B. He, Y. Kuang, Z. Hou, M. Zhou, and X. Chen, 'Enhanced electrocatalytic hydrogen evolution activity of nickel foam by low-temperature-oxidation', *J Mater Res*, vol. 33, no. 2, pp. 213–224, Jan. 2018, doi: 10.1557/JMR.2017.446.

[28] F. K. Tareq, H. Y. Lee, C. H. Shin, S. I. Kojo, and J. S. Yu, 'Honeycomb-structured S and N-codoped highly graphitized carbon as a catalyst support for Rh nanoparticles: A new benchmark electrocatalyst for hydrogen evolution reaction',

Electrochim Acta, vol. 498, p. 144627, Sep. 2024, doi: 10.1016/J.ELECTACTA.2024.144627.

[29] U. Rashid, Y. Zhu, and C. Cao, 'The comprehensive understanding of intrinsic contribution of nickel foam as a conductive substrate in water splitting', *Journal of Electroanalytical Chemistry*, vol. 973, p. 118648, Nov. 2024, doi: 10.1016/J.JELECHEM.2024.118648.

Appendices

- Calculations
- Laboratory basis
- Programming codes
- Minutes
- Etc.